Investigating the Optimal Configuration of an Interferometric Gyroscope

Authors:
Martin Opat s4704126
Luuk Elzinga s5408393
Vaggelis Atlasis s5302234
Taavi Tammaru s5333229

TA:
Amara Zahid

Course: Physics Laboratory 2

1 Abstract

Optical gyroscopes use the interference of two light beams to obtain extremely accurate information about the angular velocity [1]. Because of this, interferometric gyroscopes are used in multiple applications like navigation systems, stabilization equipment, and angular velocity sensors [2]. The aim of this experiment is to find the optimal configuration of an interferometric (or optical) gyroscope. This was done by testing different variants of the optical gyroscope using acrylic tubes, fiber-optic cables, and mirrors. By measuring the shift in light intensity when spinning the gyroscope on a rotating platform, the angular velocity Ω_{res} could be calculated. When plotting this value together with the actual Ω measured by a Raspberry Pi, we find the accuracy of each configuration. Comparing the different setups for best accuracy, price, and functionality (how easy it to was construct and align the setup), we concluded that the optimal configuration was the one of the fiber-optic gyroscope, while the mirror configuration was the least optimal as it didn't work at all. From the experimental results, the accuracy for the fiber-optic and acrylic tubes setups turns out to be somewhat equal when not accounting for outliers in the results, ((2.2 ± 0.2) rad/s and (2.1 rad/s ± 0.2) respectively using the weighted root mean squared error). The outcome was different using the median absolute percentage error which considered such values, giving an error of (27 ± 6) % for the fiber-optic gyroscope and (48 ± 5) % for the acrylic one, which matched our theoretical prediction for the relative accuracy of these two setups very well (1.68 in theory compared to our value of 1.8 ± 0.6). When considering the functionality of both setups, the acrylic tube configuration has a slight advantage over its fiber-optic counterpart but is insignificant to the advantages the fiber-optic gyroscope offers. This makes the fiber-optic gyroscope the optimal configuration of an interferometric gyroscope.

Contents

2   Introduction

Gyroscopes are devices that have existed since the mid-19th century [2] to measure orientation and angular velocity. As scientific technology advanced, innovative ways to create a gyroscope were introduced, offering various advantages and greater accuracy. Among these were different types of optical gyroscopes, the first of which appeared in the 1960s [2]. These make use of the Sagnac effect [4], a relativistic phenomenon discovered in 1913 by Georges Sagnac. A general setup consists of a laser as a focused light source and a beam-splitting mechanism to create two laser beams that will travel along the same path but in different directions toward a detector (such as a photo-resistor or photo-diode). However, rotating the setup leads to a path difference between the beams as the beam traveling along the direction of rotation travels a greater distance compared to the beam traveling in the opposite direction. Consequently, the two beams arrive at the detector in a relative phase shift - at different points in their cycle - and interfere with the amplitude of the intensity of the resultant wave depending on the phase shift. The angular velocity can be calculated by measuring the intensity of the interference pattern and comparing it to the intensity given off by the laser when the setup is stationary.

Two of the most mainstream types of gyroscope are the ring-laser gyroscope (RLG) and the fiber-optic gyroscope (FOG). The RLG was first introduced in 1963 [5] and uses mirrors to reflect the light moving through a gas medium (commonly Helium-Neon) around a triangular or square loop. Moreover, instead of using a beam splitter, the photon beams are created by applying an equal potential difference in opposite directions to the source, causing an equal number of photons to move to each direction [2]. On the other hand, the FOG was first proposed in 1976 [6] and uses fiber-optic wires as the travel medium for the laser light. The light travels along the wire through total internal reflection, which occurs at large angles when light is about to enter a less optically dense material. The main advantage of optical gyroscopes is that they have no moving parts so they remain accurate for long periods of time and are low maintenance. This is in contrast to mechanical gyroscopes, where the friction between moving components of the gyroscope - such as the wheel and the gimbals causes a decrease in accuracy over time due to the gyroscope being affected by external forces. Moreover, optical gyroscopes are incredibly accurate with state-of-the-art RLGs being able to measure rotations as low as 0.01 degrees per hour with sides only a few centimeters long [7]. Due to the above properties, they are primarily used in navigation systems for aeronautics and submarines.

For our experiment, we mainly investigated the optimal configuration for an optical gyroscope using acrylic tubes and fiber-optic wires as media for the light to travel through in the gyroscope. We judged them based on their accuracy, the range of angular velocities they can measure, and also how functional the setup is. The functionality was measured in terms of how easy it is to construct and align the setup, as well as obtain the materials necessary to do so, regarding price and availability. While we aimed to investigate air as a medium as well and managed to construct the majority of the setup, we did not manage to perform the experiment due to lacking a non-polarizing beam splitter which was an essential piece of equipment. However, an optimized configuration of the setup is discussed briefly, where the path of the laser is changed with mirrors, in a setup somewhat similar to a Ring Laser Gyroscope (RLG).

The experiment with the acrylic tubes consists of a < 1mW green laser (532 nm) which will be split into two paths by a polarizing beam splitter (PBS251). From there, the beams will follow opposite paths through the acrylic tubes ($\approx$ 16cm in length in the shape of a helix) and coincide once more at a photo-resistor which we will use to measure the light intensity using a circuit with a Raspberry Pi[1] and a 1 μF ceramic capacitor. This is done by the Raspberry Pi which measures the time taken for the capacitor to charge and discharge and returns the light intensity as a fraction of the minimum amount of time for this process to happen (for example, for high intensities this is close to 1, and for lower ones close to 0). For the second setup, we will use two < 1mW red lasers ($\approx$650 nm), which will be directly attached to 1m long fiber-optic wires (FC/PC connection, 105 μm and 125 μm diameters) with the rest of the setup remaining the same.

---

[1]The Raspberry Pi is a small computer, the size of a credit card, that can plug in a monitor and use a standard keyboard and mouse. It is very useful for connecting it to sensors. These can be programmed and used in experiments due to the small size of the Raspberry Pi which can store the data in an SD card or transmit them to a nearby device[8]

3 Theory

3.1 The Sagnac Effect

The main principle behind optical gyroscopes is the Sagnac effect. [9] To explain it, we consider a light source that emits two beams in opposite directions. These follow an identical but opposite path along a disc and arrive at their point of origin, as shown in Figure 1(a). However, when the disc starts rotating, one of the light beams travels along the direction of rotation and the other one against it (Figure 1(b)). Consequently, the two beams have different path lengths to the origin and hence arrive at different times.
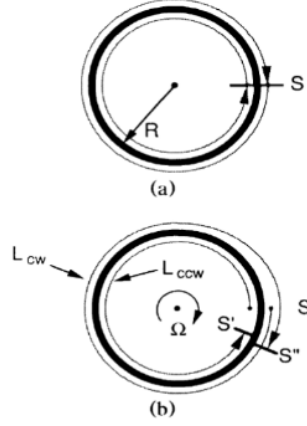

Figure 1: Counter-propagating light beams along the perimeter of (a) stationary disc and (b) rotating disc. Figure taken from [9]

A simpler analogy of this effect is its linear equivalent. When two light beams traveling in opposite directions are emitted from a moving source, if we assume the source is on a spaceship with receptors 10 meters away, one of the beams will travel more than 10 meters to the front end of the spaceship due to moving in the same direction as the receptor. Likewise, the other light beam will travel a distance shorter than 10 meters as the receptor moves toward the light ray and vice versa. As the speed of light is constant[2], the beams arrive at the corresponding receptors at a different time.

This also occurs in the Sagnac effect, with the difference being that the light waves arrive at the same point, where a receptor can be placed. Due to the difference in their paths, the two waves reach the receptor at different points in their phase, changing the intensity of light received. We can calculate this change using the following derivation.

The path length of the light beam in the counterclockwise and clockwise directions is given by equations:

$$L_{ccw} = 2\pi R - R\Omega t_{ccw} = ct_{ccw} \tag{1}$$

$$L_{cw} = 2\pi R + R\Omega t_{cw} = ct_{cw} \tag{2}$$

where

$$L_{ccw} - \text{light path length (counterclockwise)}$$
$$t_{ccw} - \text{light path duration (counterclockwise)}$$
$$L_{cw} - \text{light path length (clockwise)}$$
$$t_{cw} - \text{light path duration (clockwise)}$$
$$R - \text{radius of rotation}$$
$$\Omega - \text{angular speed (setup)}$$
$$c - \text{the speed of light}$$

This length is equal to the circumference of the disc plus (minus) the distance the disc moves in a given time $R\Omega t_{ccw}$ ($R\Omega t_{ccw}$) (note that s = vt and v = ω R).

---

[2]The value of the speed of light changes in media with a different refractive index due to refraction. However, when performing calculations the refractive index cancels out and does not influence the results of the experiment [9]

Re-arranging the two equations for the time in terms of the path length and the speed of light, we find the time difference between the two beams traveling an identical path length which we can write in terms of the variables above as:

$$\Delta t = t_{cw} - t_{ccw} = \frac{2\pi R \cdot 2R\Omega}{c^2} = \frac{4\pi R^2 \Omega}{c^2} \tag{3}$$

$$\Delta L = c\Delta t = \frac{4\pi R^2}{c}\Omega \tag{4}$$

$$\tag{5}$$

where

$$\Delta L - \text{Difference in paths' lengths}$$
$$\Delta t - \text{difference in paths' duration}$$

Finally, the phase difference between the light wave functions, Φ is given by

$$\Phi = \frac{2\pi}{\lambda}\Delta L = \frac{8\pi^2 R^2}{\lambda c}\Omega \ [9] \tag{6}$$

It can be shown [9] that the above formula holds for any medium. The formula can also be transformed into a general form of

$$\Phi = \frac{8\pi A}{\lambda c}\Omega \tag{7}$$

, where A is simply the area enclosed by the path of the two light rays. In the case of a coil, this formula can be even further transformed as:

$$\Phi = \frac{2\pi LDn}{\lambda c}\Omega \tag{8}$$

,where L is the length of one loop of the coil, D is the diameter of the coil and n is the number of turns of the coil.

Next, we can calculate the effect this phase difference will have on the amplitude of the light waves. Modeling the light waves as cosine waves with amplitude A_0, the light intensity at a given point is found by superposing the two waves together, given by:

$$\frac{A_0}{2}\cos\left(\omega t + \Phi\right) + \frac{A_0}{2}\cos\left(\omega t\right)$$

where

$$A_0 - \text{light wave amplitude}$$
$$\omega - \text{light wave angular frequency}$$
$$\Phi - \text{difference in phase of light wave function}$$
$$t - \text{time}$$

These are identical cosine waves shifted Φ radians apart. By shifting our frame of reference by $-\frac{\Phi}{2}$ radians we end up with an equation that is symmetrical with respect to the y-axis:

$$\frac{A_0}{2}\cos\left(\omega t + \frac{\Phi}{2}\right) + \frac{A_0}{2}\cos\left(\omega t - \frac{\Phi}{2}\right)$$

From there, we can simplify the expression into one wave more elegantly than in the previous reference frame as shown below ($\Re$ indicates the real component of the expression in the curly brackets):

$$\frac{A_0}{2}\cos\left(\omega t + \frac{\Phi}{2}\right) + \frac{A_0}{2}\cos\left(\omega t - \frac{\Phi}{2}\right)$$

Using Euler formula for cosine we can write

$$\frac{A_0}{4}\Re\left\{e^{i\left(\omega t+\frac{\Phi}{2}\right)}+e^{-i\left(\omega t+\frac{\Phi}{2}\right)}\right\}+\frac{A_0}{4}\Re\left\{e^{i\left(\omega t-\frac{\Phi}{2}\right)}+e^{-i\left(\omega t-\frac{\Phi}{2}\right)}\right\}$$

The real component of the complex exponential is equal to its complex conjugate so we can simplify the expression into

$$\frac{A_0}{2}\Re\left\{e^{i\left(\omega t+\frac{\Phi}{2}\right)}+e^{i\left(\omega t-\frac{\Phi}{2}\right)}\right\}$$
$$\frac{A_0}{2}\Re\left\{e^{i\,\omega t}\left(e^{i\frac{\Phi}{2}}+e^{-i\,\frac{\Phi}{2}}\right)\right\}$$
$$A_0\cos\left(\omega t\right)\cos\left(\frac{\Phi}{2}\right)$$

Switching back to the original reference frame by adding $\frac{\Phi}{2}$ radians we obtain:

$$A_0\cos\left(\omega t\right)\cos\left(\Phi\right)$$

We also account for a possible default path difference α due to the setup and end up with:

$$A_0\cos\left(\omega t\right)\cos\left(\Phi+\alpha\right) \tag{9}$$

Note that we will attempt to minimize the value of α as much as possible in our experiment. However, our setup is not able to measure the wave function, only the intensity I. We know that:

$$I\propto|A|^2=|A_0\cos\left(\Phi+\alpha\right)|^2\;[10]$$

Thus, we can finally write:

$$I=I_0\cos\left(\Phi+\alpha\right)^2 \tag{10}$$

3.2   Theory Behind the Function of Electronic Components

The Raspberry Pi in the circuit measures the intensity as a fraction of how fast the capacitor charges/discharges. For a capacitor at initial charge Q_0, the charge, Q, at a given point in time, t, is given by [11]:

$$Q=Q_0 e^{\frac{-t}{RC}} \tag{11}$$

with R denoting the resistance of the photo-resistor in the circuit and C the capacitance of the capacitor. Re-arranging the equation for t:

$$t=RC\ln\left(\frac{Q_0}{Q}\right) \tag{12}$$

A photo-resistor is a variable resistor made out of semiconducting material. The resistance of the component is inversely proportional to the light intensity shone on the component. Hence, for greater light intensity, the resistance of the photo-resistor and the total resistance in the loop decreases, causing a greater current to flow through the components in that loop.[3]

---

[3]The phenomenon behind this is related to the properties of semiconductors and is explained by a concept called band theory [12]. However, understanding it is not necessary for the purposes of the experiment and it is sufficient to have a surface understanding of the function of a photo-resistor.

3.3   Optics Relevant to the Experiment

In the two variants of our experiment, light traveled through acrylic tubes and fiber-optic wires. In both cases, it reached the boundary between media many times, e.g. acrylic and air, in the case of the acrylic tubes. At these boundaries, the light follows the fundamental laws of geometric optics depending on the angle of incidence between the light ray and the normal to the surface.

The first law of reflection states that the incident, reflected, and transmitted rays form a plane. This plane is shown in Figure 2 and is called the plane of incidence. From this plane, the p-polarization and s-polarization are defined [11]. The polarization vector defines the direction in which the electric field of the light wave oscillates. Waves that are polarized in the plane of incidence are said to be p-polarized. On the other hand, waves that oscillate perpendicular to the plane of polarization are called s-polarized.
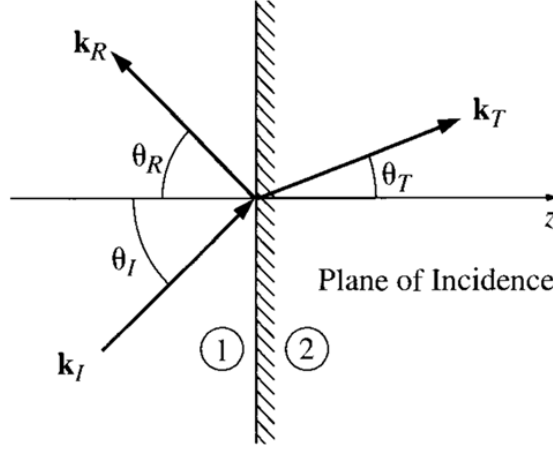
$$n_1 \sin(\theta_I) = n_1 \sin(\theta_R) = n_2 \sin(\theta_T)$$

Figure 2: Diagram showing a light ray at a boundary between two materials (1 and 2) where we can see the three light rays forming the plane of incidence. The vector k denotes the direction of propagation of each ray and θ the angle to the normal for the incident (I), reflected (R), and transmitted (T) rays. Finally, n_1 is the refractive index for material 1, and n_2 is the refractive index for material 2. Figure obtained from [11]

The second law of reflection states the angle of reflection, θ_T is equal to the angle of incidence θ_I.
The third law of reflection (also known as Snell's law), states:

$$n_1 \sin \theta_I = n_2 \sin \theta_T \tag{13}$$

where all quantities remain the same as in the figure above. To further specify, n_1 and n_2 denote the refractive index of each material, defined by the fraction of the speed of light in vacuum at which light moves inside the material ($n = \frac{c}{v}$ where v is the speed of light in the material and c the speed of light in vacuum. Note that $v \leq c$).

At boundaries where light is moving from a more optically dense to a less optically dense material ($n_1 ¿ n_2$) it is possible for the angle of transmission to be 90 degrees, with the light traveling along the boundary. This angle is called the critical angle θ_C and is given by re-arranging equation 13 for θ_T:

$$\sin \theta_C = \frac{n_2}{n_1}$$

For all angles greater than the critical angle, no light will be transmitted and all of it will be reflected back into the material.

4 Methods

4.1 Experimental Setup

4.1.1 Fundamentals of the Experiment

The parts common to all three experimental setups are the rotating base and photo-resistor circuit. The base, a diagram of which is shown in Figure 3, consisted of a 35cm round styrofoam plate that was mounted onto a piece of rotating apparatus rigid enough for the base to be stable and well supported. In our case, this was done with a rotating chair from the lab and construction-grade duct tape to keep the platform in place. While not the most scientific mechanism for a rotating platform, the chair had a large radius and provided a practical way to rotate the base around the central axis.

All the experiments were performed in the optics room in a dark setting. This allowed us to see where the laser beam travels and if there was any leakage of light in the acrylic tubes or fiber-optic cable. During the experiment, the room doesn't in fact need to be completely dark; it is more important that the background lighting is constant so that the only change in light intensity comes from the rotation of the platform.

Applying torque to the plate can be achieved by using a DC motor that unwinds a string rolled around the leg of the rotating platform, or by having the DC motor make contact with the perimeter of the circular base of the gyroscope and rotate it in a gear-like motion. Since the rotation does not in principle need to be constant in order to test the gyroscope setups, the initial torque can be given by a hand. This provides the advantage that we can test the set-ups over a range of angular velocities, as well as how well the setups respond to changes in the angular velocity of the system (which inherently occurred due to friction in the components of the chair, in a scenario closer to the real world applications of the instrument)
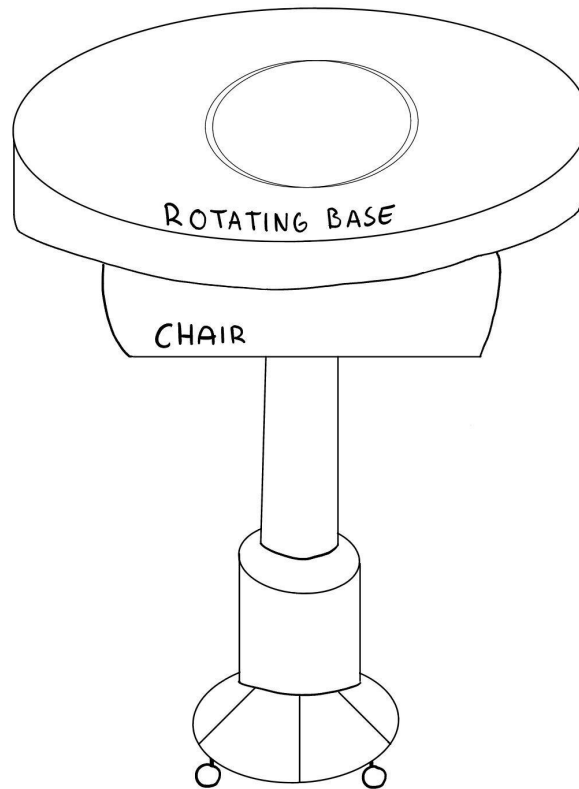

Figure 3: Diagram of the gyroscope base showing the Styrofoam plate mounted on top of the chair. The platform was held in place using several pieces of duct tape which were attached to the plate and chair.

4.1.2 Light Sensor Circuit

In order to collect the data, a photo-resistor and a 1 μF capacitor were mounted to a breadboard in series; in turn, this was connected to a Raspberry Pi computer, as shown in Figure 4. Finally, the Raspberry Pi was connected to a power-bank so it could operate and transmit data during the rotation. In some setups, the

power-bank - which weighed approximately 450g - had to be placed far from the center of the platform so we added counterweights on the opposite side of the base to keep the center of mass of the system as close to the center as possible.
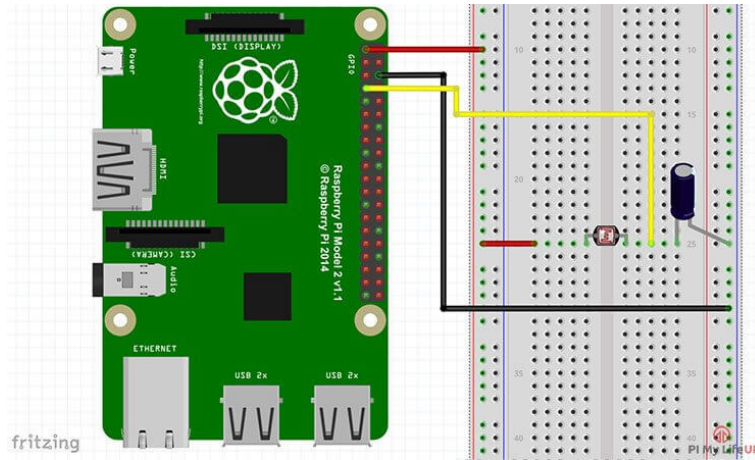

Figure 4: Circuit diagram which shows the Raspberry Pi connected to a circuit with the photo-resistor and capacitor in series. The wire in between them represents the connection where the voltage is measured, equivalent to placing a volt meter between this position and the ground (the black wire in the diagram). Diagram from [13]

The resistance of the photo-resistor we used is inversely proportional to the light intensity. Hence, for greater light intensities the current going through the photo-resistor increases. This current charges the capacitor in a time-dependent on its capacitance and the resistance of the photo-diode. The Raspberry Pi records the time it took for the capacitor to charge/discharge and calculates the light intensity as a decimal with reference to the minimum amount of time taken for this process to occur, which was represented by 1. Therefore, an increase in the current flowing through the capacitor (which was connected in series to the photo-resistor) led to it being charged up faster.

Moreover, the Raspberry Pi also has its own internal gyroscope which measures acceleration in the roll, pitch, and yaw axes [14] a diagram of which is shown in Figure 5. This allows us to compare our experimental data with the true rotational velocity of the Raspberry Pi and, therefore, the platform.
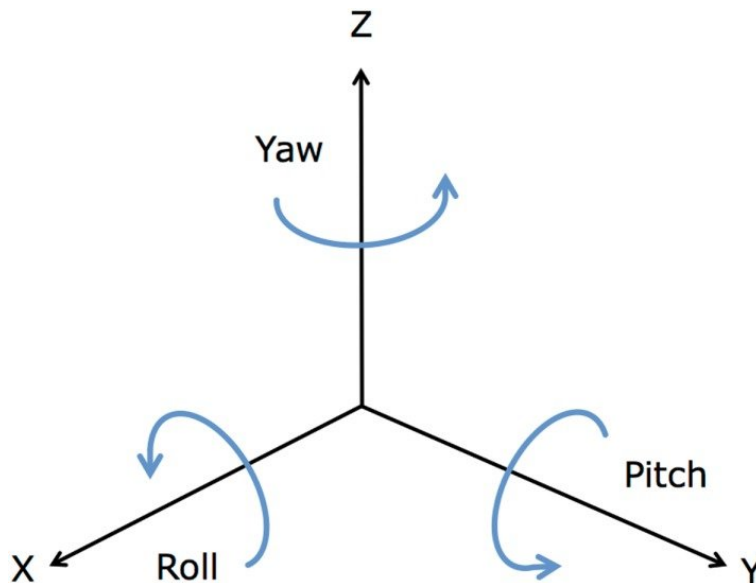

Figure 5: Diagram displaying how the roll, pitch, and yaw axes are defined in a three-dimensional plane. Figure taken from [15]

4.1.3 The Acrylic Tube Variant

In the first variant of the gyroscope, we used acrylic as a travel medium for the light in the form of two identical helix-shaped acrylic tubes. The tubes, which were actually optical fiber models, were approximately 57 cm long. Due to the shape, these formed a 10 cm x 10 cm square area. In the setup shown in Figure 6, we used a square polarizing beam splitter (model PBS251 from THORLABS, with 2.54 cm sides made from a type of glass called N-SF1) for the wavelength range 420 nm - 680 nm, to split the laser light (532 nm, 2 mm in diameter, power ¡ 1mW) into the acrylic tubes. [4]. These acrylic tubes guided the light beam through two separate paths to the photo-resistor, thus creating a situation where light has to travel against the rotation of the platform in one path and with the rotation in the other path.

The polarizing beam splitter split the light from the laser into two beams with orthogonal polarizations. In the middle of the beam splitter, there is a boundary between the glass the beam splitter is made of and the glue that keeps the two triangular prisms that make up the splitter together. This boundary runs across the diagonal and is designed to reflect incident light that is s-polarized by 90 degrees and let through p-polarized light. In our experiment, the three rays form a horizontal plane so the transmitted beam was polarized horizontally and the reflected beam was polarized vertically. In our case the beam splitter had an extinction ratio of 1000:1, meaning that a much more significant portion of the light got transmitted and a small portion got reflected. Thus the light intensity in one tube was noticeably stronger, which should be taken into account during data processing.

The acrylic tubes were then placed such that the incident light is perpendicular to the normal of the end of the tube. Due to the irregular shape of the tube, light reached the acrylic-air boundary numerous times, where most of the light then underwent total internal reflection from the side of the tubes. It then exited the tube from the other ends, slightly less focused due to the greater radius of the tube (1cm) and the scattering that occurred inside the tube due to total internal reflection. However, this had little consequence on our results as it was only the intensity of the beams shining on the photo-resistor that was of interest.
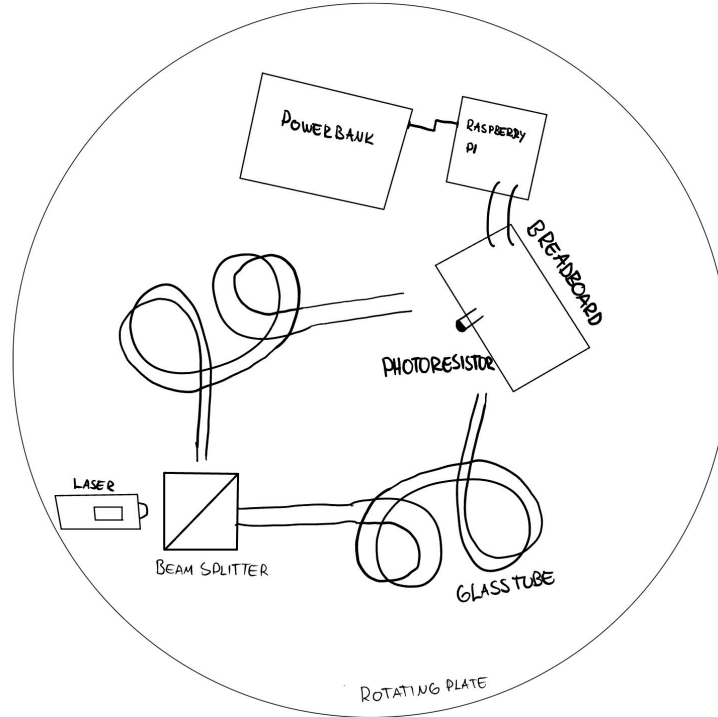

Figure 6: Diagram of acrylic tube gyroscope setup. The acrylic tubes used had the shape of a helix, hence their unconventional shape in the diagram. The line across the beam splitter indicates that a fraction of the beam moves straight through the beam splitter, whilst the other fraction is reflected by 90 degrees towards the other tube.

---

[4]Ideally, the beam splitter should be non-polarizing to keep the calculations as simple as possible. However, we did not have access to one and instead measured the polarization of the beam and calculated the effect this had on our results, finding the rotational velocity accordingly

4.1.4 The Fiber-optic Cable Variant

In the second variant of the gyroscope, two identical lasers were used that were directly connected to fiber optic cables 1m long, manufactured for a range of wavelengths between 633 nm - 780 nm. Each fiber optic cable (diameters 105 μm and 125 μm) completed 1.35 turns and then pointed towards the photo-resistor, after going through some polarizing paper so that both beams oscillated in the same direction - otherwise little to no interference occurs. For this variant two identical lasers (2mm diameter, power ¡ 1mW) with wavelengths between 620 nm - 680 nm were used, eliminating the need for a beam splitter. Additionally, these lasers were battery-powered so there were no cables that would interfere with rotating the setup.

These fiber-optic cables represented a medium more commonly used in modern optical gyroscopes compared to acrylic. The fiber-optic cable consists of many thin wires of plastic called optical fibers. These optical fibers make up the core of the cable which is surrounded by the cladding layer. Total internal reflection occurs between these two layers, similar to acrylic but more effective as the ratio between the refractive indices of the fiberglass and the cladding makes the critical angle smaller.

The fiber-optic cables were set to be as close to a perfect circle as possible and held in place one on top of the other using 3D-printed holders to minimize the path difference. The circle of cables had a diameter of 23.5cm and was carefully placed to be concentric with the axis of rotation to ensure that the respective light paths move equally with and against the rotation.

Right where the laser light exited the fiber-optic cable, a polarizing paper was placed. This only lets through light with polarization in a single direction. This was necessary in order for the beams to be able to efficiently interfere, as non-polarized light interferes in all (infinitely many) planes of polarization. In some planes of polarization, this interference is constructive while in others it is destructive. On average, however, these effects cancel out and the overall intensity remains unchanged.
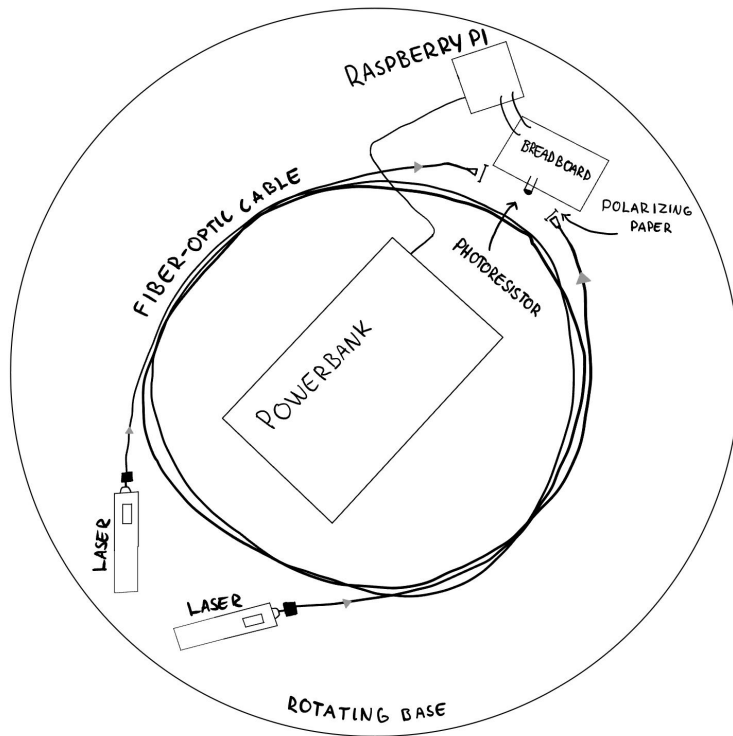

Figure 7: Diagram of the fiber-optic variant of the gyroscope. Two lasers were attached to the fiber-optic cables which formed two circular paths, with the other end pointing at the photo-resistor.

4.1.5 The Mirror Variant

In the third variant of the experiment, the acrylic tubes were substituted for 3 mirrors[5]. The mirrors along with the beam splitter formed a square path 15 cm long for the beam to follow (Figure 5). The mirrors were mounted onto 3D-printed mirror stands that offered crucial stability to keep the optical alignment when the whole base is rotating. The photo-resistor was placed behind the beam splitter, in the opposite direction to the path of the beams. During alignment, the mirrors were placed and oriented such that the light from both paths coincided with the mirrors and beam splitter at the same point, allowing for the photo-resistor to absorb both beams.
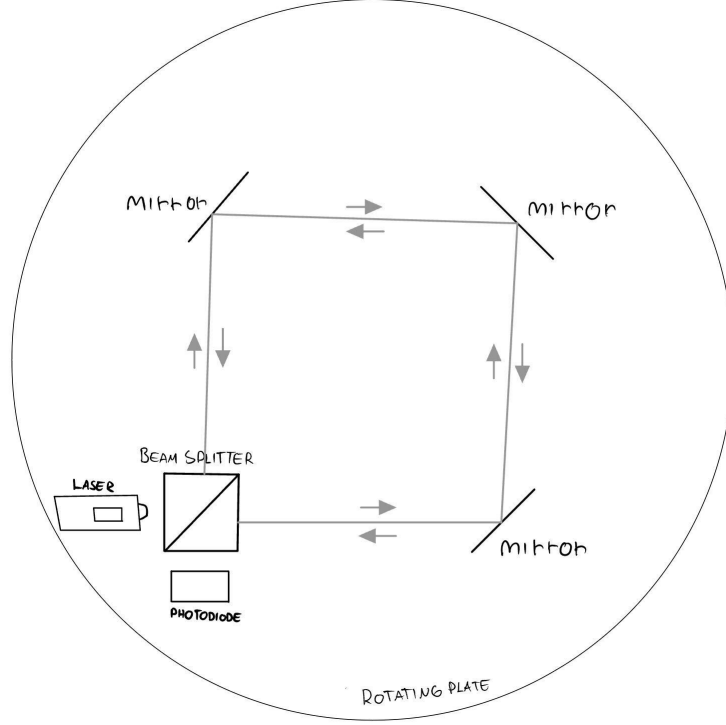

Figure 8: Diagram of mirror gyroscope setup. Can be achieved by placing the mirrors adjacent to the beam splitter at an equal distance from it and oriented such that the angle of incidence is 45 degrees. The alignment is completed by fine-tuning the setup such that the two laser beams fall on top of each other at the photo-resistor.

4.2 Method for Data Collection

We set out to do at least three sets of runs with each type of configuration of the setup. Each set consisted of a stationary run, to test the alignment of the setup and a run where we spun the rotating platform by exerting an impulse on it. Due to the friction between the component of the chair, the rotational velocity was not constant but rather slowed down gradually. This allowed us to measure how accurately our setup responds to changes in the rotational velocity of the platform.

The path lengths may not be exactly the same in our experiment, which might change the light intensity. Thus, an additional run should be performed in order to find the base ground of the intensity for a stationary setup, we can call this run a configuration run. During a predetermined time interval of 40 seconds, the Raspberry Pi collected data of the light intensity using the method corresponding to each setup. A live feed of the data was visible in the console in order to make quick corrections to the setup if something appeared to be malfunctioning. The data was afterward stored in a compact file for further analysis, as well as uploaded into the `data` folder in the code's repository 9.1.1.

---

[5]This setup required a non-polarizing beam splitter, as the two beams were perpendicularly polarized so they did not interfere. Consequently, a description of the setup we constructed is provided below but no results were collected for this version of the experiment

4.3   Data processing methods

4.3.1   The Fiber-optic Cable Variant

In this variant of the setup, the phase shift α caused by the unequal light paths is negligibly small. As such, equation 10 can be used with $\alpha = 0$ in order to determine the phase shift Φ caused by the Sagnac effect. The value of I_0 is directly measured when the setup is stationary, and thus the calculated Ω_{res} can be obtained simply from equation 8.

4.3.2   The Acrylic Tube Variant & The Mirror Variant

In these two variants of the setup, the phase shift α caused by the unequal light paths is not negligible and needs to be taken into account. This means, that at least one configuration run needs to be taken. This configuration run is then used for calibration, where the exact value of α can be determined. This is done by fitting the plot of measured intensity I against the true rotational speed Ω of the setup.

Due to the non-zero value of α, the value of I_0 is not (necessarily) measured when the setup is stationary. In reality the measured intensity I_{start} measured during a stationary run is given by modified equation 10 for $t = 0$:

$$I_{stat} = I_0 \cos^2 \alpha \Rightarrow I_0 = \frac{I_{stat}}{\cos^2 \alpha}$$

Knowing the value of α, however, allows us to also calculated the value of I_0 by using the above equation. After all these extra steps, the same two theoretical equations (7, 10) can be used in order the obtain Ω_{res}.

4.4   Method Evaluation

To evaluate how close the Ω calculated from equation 6 matches the true Ω measured by the Raspberry Pi, two statistical quantities are used and their values are compared across different setups. Specifically, the first quantity is the median absolute percentage error [16] which isn't sensitive to outliers or data errors. The second quantity is the weighted root mean square error [17] which is sensitive to outliers and data errors.

Using the information we know about the two setups, we can come up with a theoretical prediction for the ratio of their accuracy. Using equation 7, we know that for a given angular velocity the phase shift is proportional to the enclosed area divided by the wavelength of the laser light. We can then use the ratio of the phase shifts for a given angular speed to approximate the ratio of their accuracy. For the acrylic setup, the area enclosed was 0.01 m^2 with a 40 cm square perimeter. Knowing the total length of the acrylic tubes was 1.14 m, we can approximate the number of turns around this rectangle to be 3.8 (and therefore approximate the effective enclosed area to be 0.019). On the other hand, the fiber-optic setup was circular with 1m long cables in a circle with a 23.5 cm diameter and 1.35 turns (1 m length divided by the circumference, π x the diameter). We will approximate the accuracy of the gyroscope based on how big the phase shift is for a given angular velocity. Recall, that lasers had wavelengths of $532x10^{-9}m$ and $650x10^{-9}m$. We can then use equation 7 to show that in the acrylic setup, $\phi = (4.49x10^{-3})\Omega$ and in the fiber-optic setup, $\phi = (7.55x10^{-3})\Omega$. Dividing the latter by the former, we expect ϕ to be 1.68x greater for the fiber-optic gyroscope and therefore to be 1.68x more accurate.

5 Results

All the raw data, as well as the graphs and the code, used in all experiments can be found in the designated public GitHub repository 9.1.1. These include graphs of rotational speed as a function of time which are obtained from the internal gyroscope of the Raspberry Pi and are used for the evaluation of each variant of the setup. All other graphs are used and obtained for the data processing itself.

5.1 Comparing the Setups Using the Median Absolute Percentage Error (MAPE)

In Table 1 the exact values of MAPE for each successful trial are shown for two setups, along with the mean and standard error in the mean of MAPE across these trials. From the table, we can see that the fiber-optic variant, MAPE of $(27 \pm 6)\%$, is significantly more accurate in comparison with the acrylic tube variant, MAPE of $(48 \pm 5)\%$. These values were obtained in data processing performed in Python which directly calculated the values of MAPE.

Here, we divide the error of one setup (acrylic) by the other (fiber-optic) and find the relation between them to be ≈ 1.78 (48/27). To calculate the range of values this could lie in we consider the errors from each setup and divide the maximum of the acrylic setup by the minimum of the fiber-optic and vice versa, subtracting and dividing by 2 to conclude that the fiber-optic setup is (1.8 ± 0.6)x more accurate than the acrylic one. The result matches our theoretical prediction very well.

SetUp	Median absolute percentage error (%)					Standard Error in the Mean (%)
	Trial 1	Trial 2	Trial 3	Trial 4	Mean	
Fiber-Optic Cables	26.48	40.12	31.88	10.11	27	6
Acrylic Tubes	52.96	55.02	44.99	37.55	48	5

Table 1: Table displaying the values of median absolute percentage error for different runs of the two setups

5.2 Comparing the Setups Using the Weighted Root Mean Squared Error (WRMSE)

In Table 2 the exact values of WRMSE for each successful trial are shown for two setups along with the mean and standard error in the mean of WRMSE across these trials. From the table, we can see that both variants performed similarly well. WRMSE of fibre-optic setup variant is (2.2 ± 0.2) rad/s, and WRMSE of acrylic tubes setup variant is (2.1 ± 0.2) rad/s.
These values were obtained in data processing performed in Python which directly calculated the values of WRMSE.

Using the same method as for the Median Absolute Percentage Error, we obtain an accuracy ratio of 1.0 ± 0.2, indicating the accuracy of the two setups is the same, a result which is far off what we expected.

SetUp	Weighted root mean squared error (rad / s)					Standard Error in the Mean (rad / s)
	Trial 1	Trial 2	Trial 3	Trial 4	Mean	
Fiber-Optic Cables	2.69	2.54	2.39	1.25	2.2	0.2
Acrylic Tubes	2.63	2.47	1.55	1.27	2.1	0.2

Table 2: Table displaying the values of weighted root mean squared error for different runs of the two setups

5.3 Comparing the Setups Regarding Price and Functionality

When looking at the total price of the setups mentioned below, we only considered the parts which had a significant financial impact.

5.4 The Acrylic Tube Variant

The acrylic tube method yielded approximations of the rotational speed that were accurate enough to consider the gyroscope functional. The actual rotational speed was obtained from the Raspberry Pi by measuring the rotation around the yaw axis. With the equations 10) the graph of rotational speed against time was obtained from the data of intensity against time. The phase shift was calculated using equation 6. The figure 9 below show the graphs of true Ω, intensity, calculated Ω_{res}, and phase shift for the most successful run out of 49 functional runs across multiple days. The same set of graphs for two additional successful runs are added to

Acrylic tube	Fiber-optic cable
Green laser(532nm): €300	2x Red Laser(620-680nm): €200
Beam splitter: €230	2x Fiber-optic cable: €50
2x acrylic tubes: €50	-
Raspberry Pi + circuit: €130	Raspberry Pi + circuit: €130
Styrofoam base: €15	Styrofoam base: €15
Total: €735	Total: €415

Table 3: Prices of individual parts and their total sum across the fiber-optic cable setup variant and acrylic tubes setup variant.

the appendix, section 9.3.1.
Figure 10 shows the overall accuracy of the calculated omega by putting it side by side with the true omega. From the graph, it is evident that the calculated omega is a good approximation of true omega even though it fluctuates considerably and becomes inaccurate below 2 rad/sec.
Figure 11 is the fitted graph of the configuration run and is used to calculate the phase shift α, which in this case had the value of $\alpha = (-0.43 \pm 0.01)$rad.

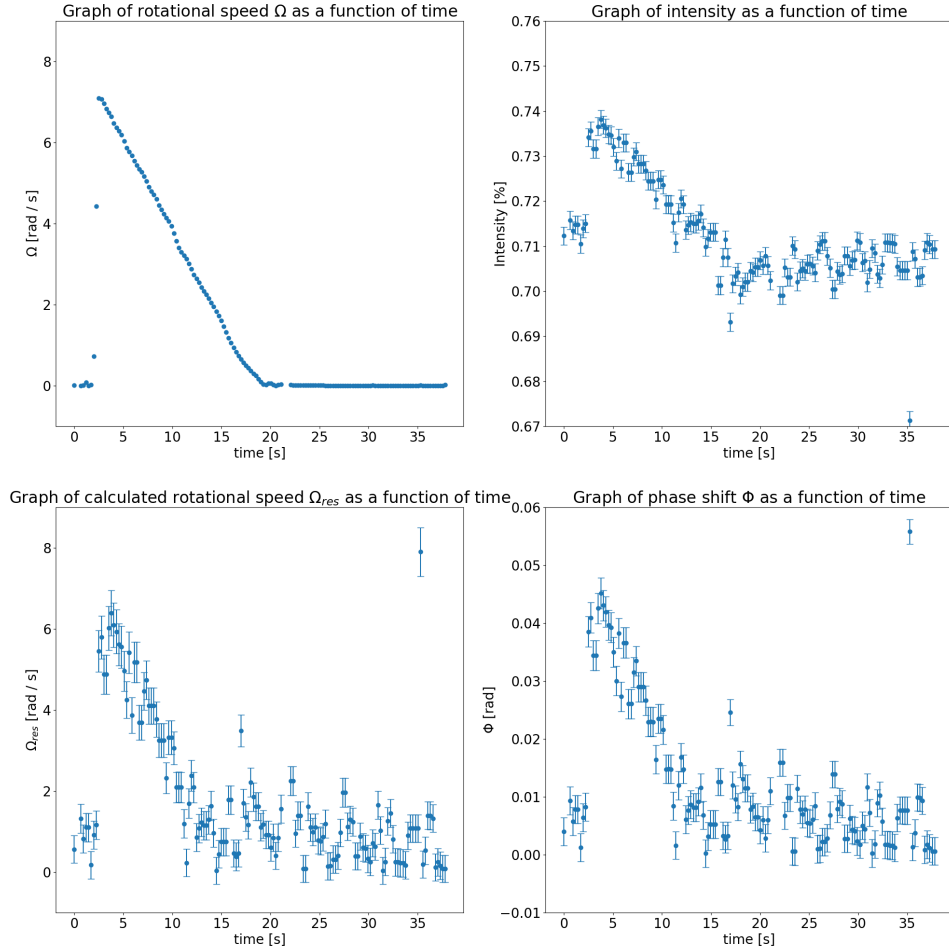### Graphs for one complete measurement using acrylic-tubes setup (run=10)

Figure 9: The graphs of rotational speed measured by the Raspberry Pi, intensity measured by the photo-resistor, rotational speed calculated from the intensity, and phase shift of the light from run number 10 of the acrylic tubes variant.
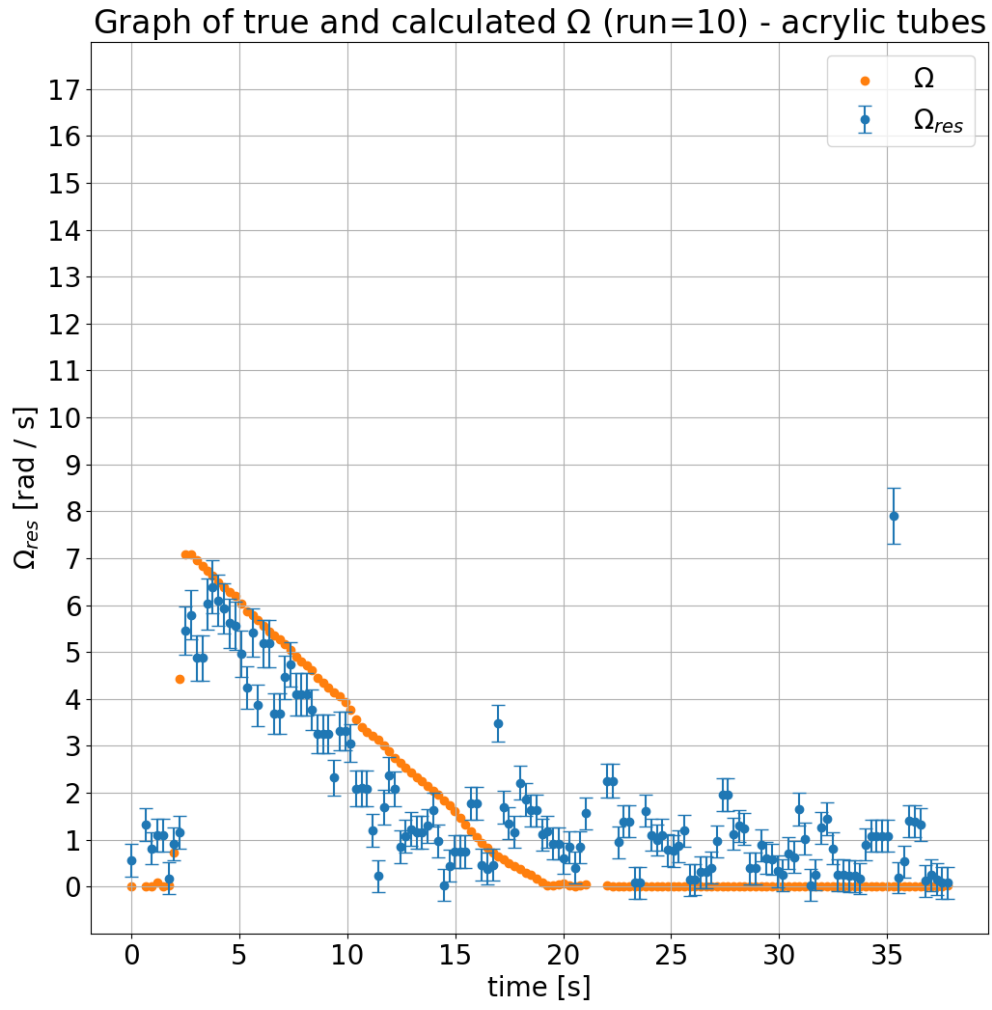
Figure 10: The comparative graph of the true omega (orange) and the omega calculated from intensity(blue) against time for the run number 5 of the acrylic tubes variant
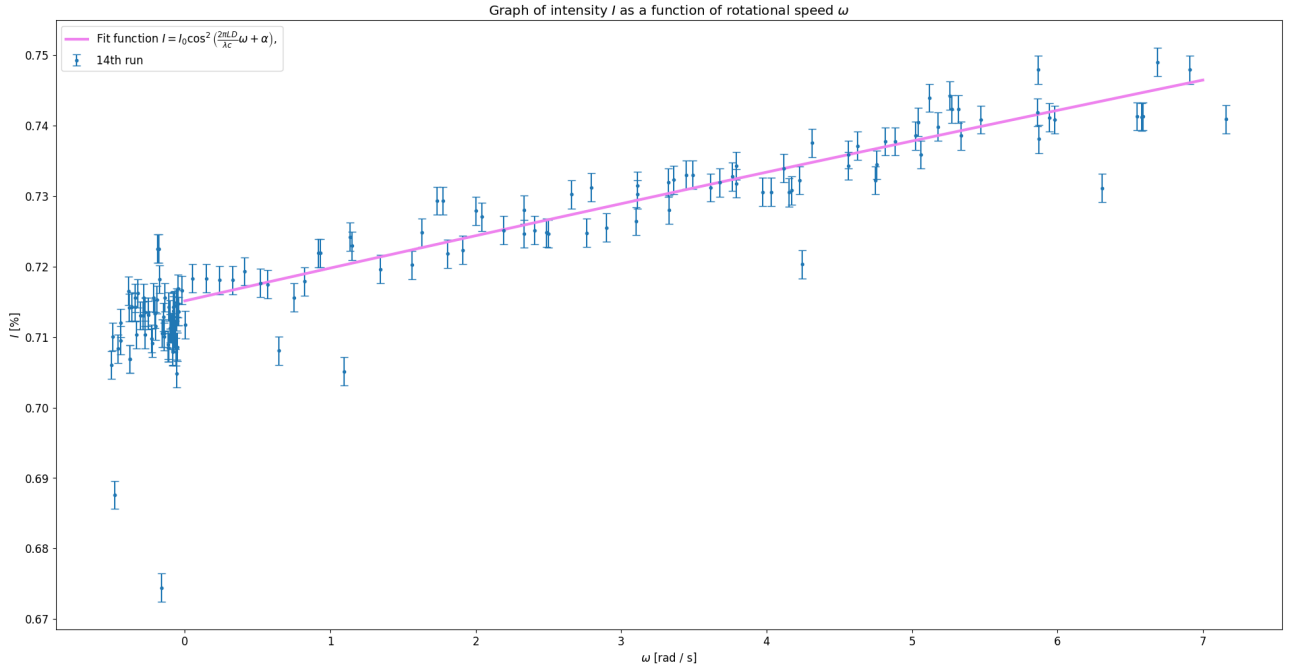
Figure 11: Graph of light intensity against true Ω and a best fit line to phase shift α from

5.5 The Fiber-Optic Cable Variant

This method yielded the most accurate approximation of the rotational speed. Like in the previous variant, the true rotational speed for the fiber-optic cable variant was obtained from the Raspberry Pi by measuring the rotation around the yaw axis. In this case, the rotational speed was measured only up to 10 rad/s. For the three runs included in the report, this fact didn't make it difficult to understand the trend and the overall shape of the graph because the value of 10 rad/s was exceeded only for a few seconds. The actual Ω could still be compared to the Ω_{res} calculated from the light intensity. With the equations 10) the graph of rotational speed against time was obtained from the data of intensity against time. The calculated intensity was visibly a valid approximation of the actual intensity. Although it had some additional oscillations due to the slight instability of the setup. The phase shift was calculated using equation 8.

Below the figure 12 shows the graphs of true Ω, intensity, calculated Ω_{res}, and phase shift Φ for the most successful run out of 26 functional runs across two days. The same set of graphs for two additional successful runs are added to the appendix, section 9.3.2.

Figure 13 shows the overall accuracy of the calculated omega by putting it side by side with the true omega. From the graph, it is evident that the calculated omega is a good approximation of true omega even though it fluctuates considerably and becomes inaccurate below 1 rad/sec.

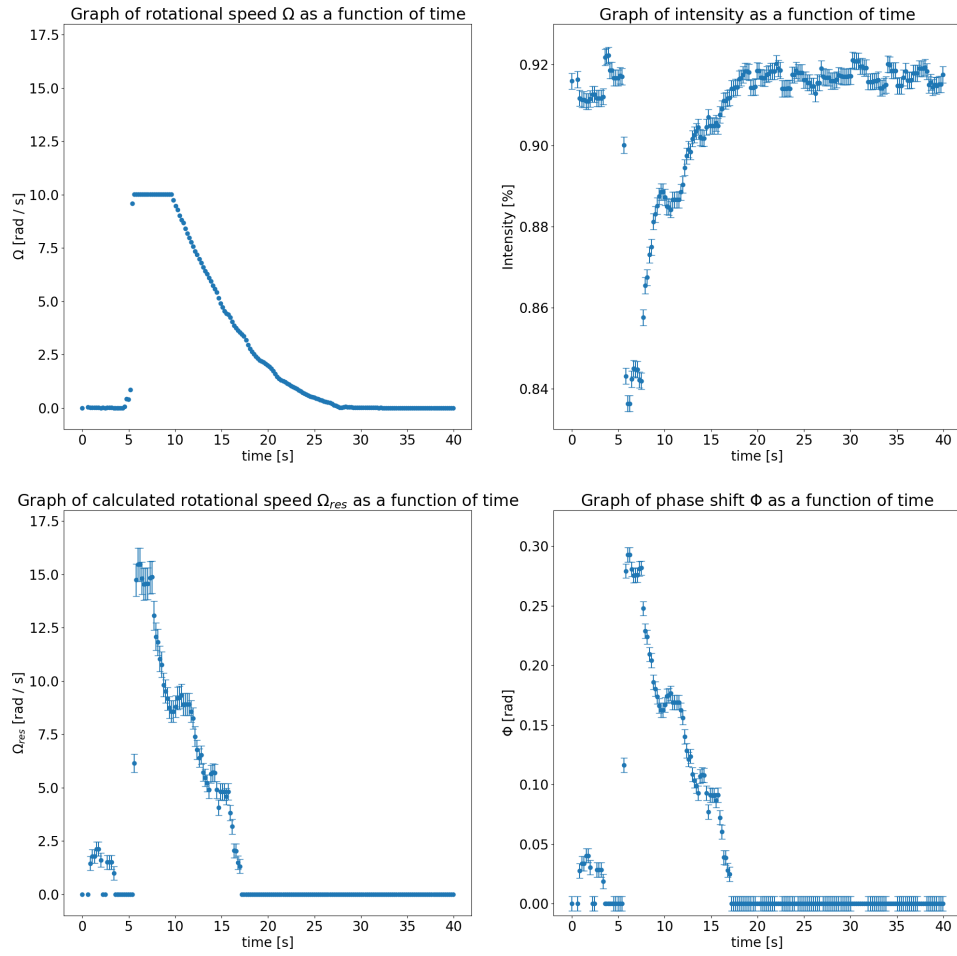# Graphs for one complete measurement using fibre-cables setup (run=23)

Figure 12: Graphs of rotational speed measured by the Raspberry Pi, intensity measured by the photo-resistor, rotational speed calculated from the intensity, and phase shift of the light from run number 23 of the fiber-optic variant.
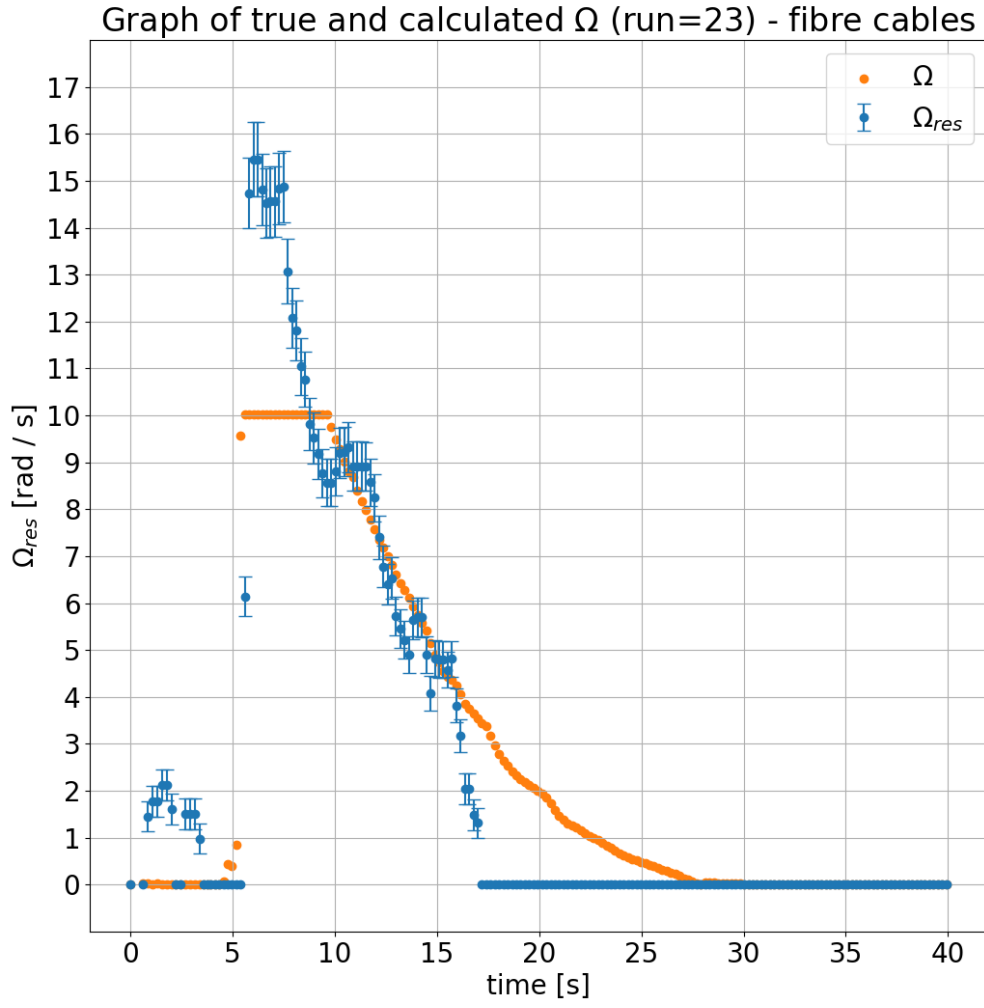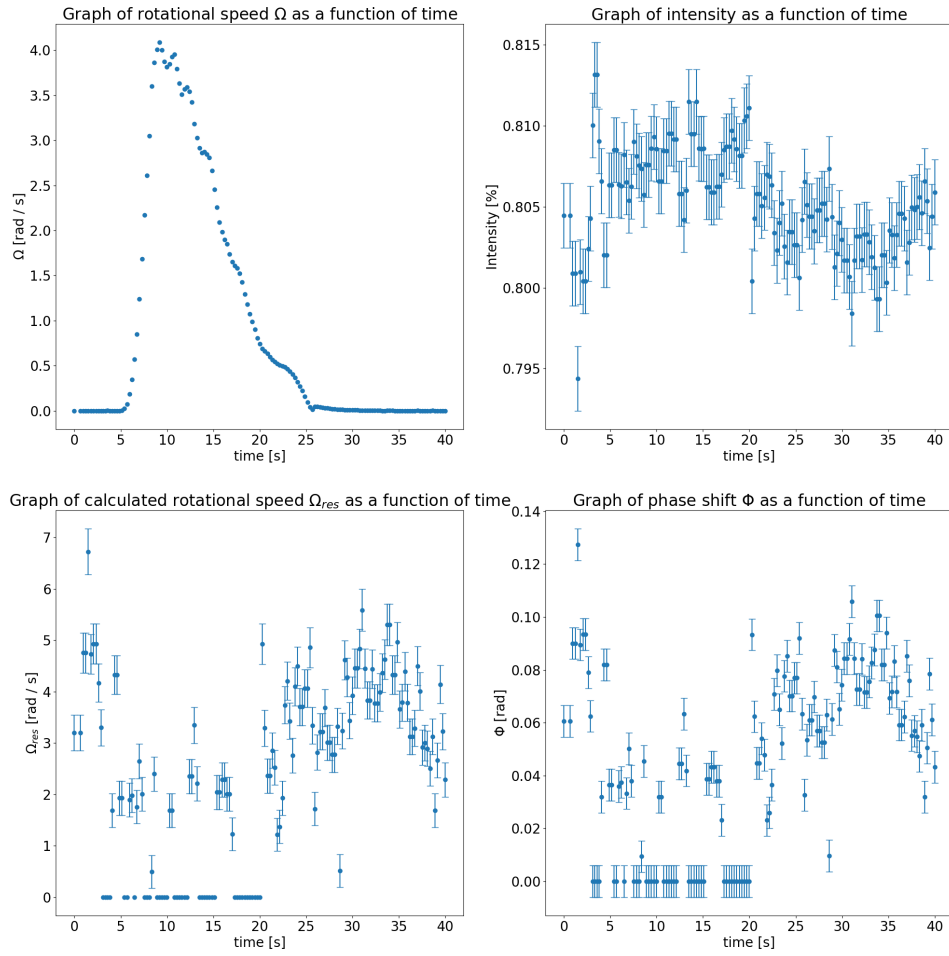
Figure 13: The comparative graph of the true omega(orange) and the omega calculated from intensity(blue) against time for run number 17 of the fiber-optic variant.

5.6 The Mirror Variant

As can be seen in figures 14 and 15 below, the mirror setup variant did not follow the same trends as the other two variants.

Figure 14: The graphs of rotational speed measured by the Raspberry Pi, intensity measured by the photo-resistor, rotational speed calculated from the intensity, and phase shift of the light from run number 8 of the mirror setup.
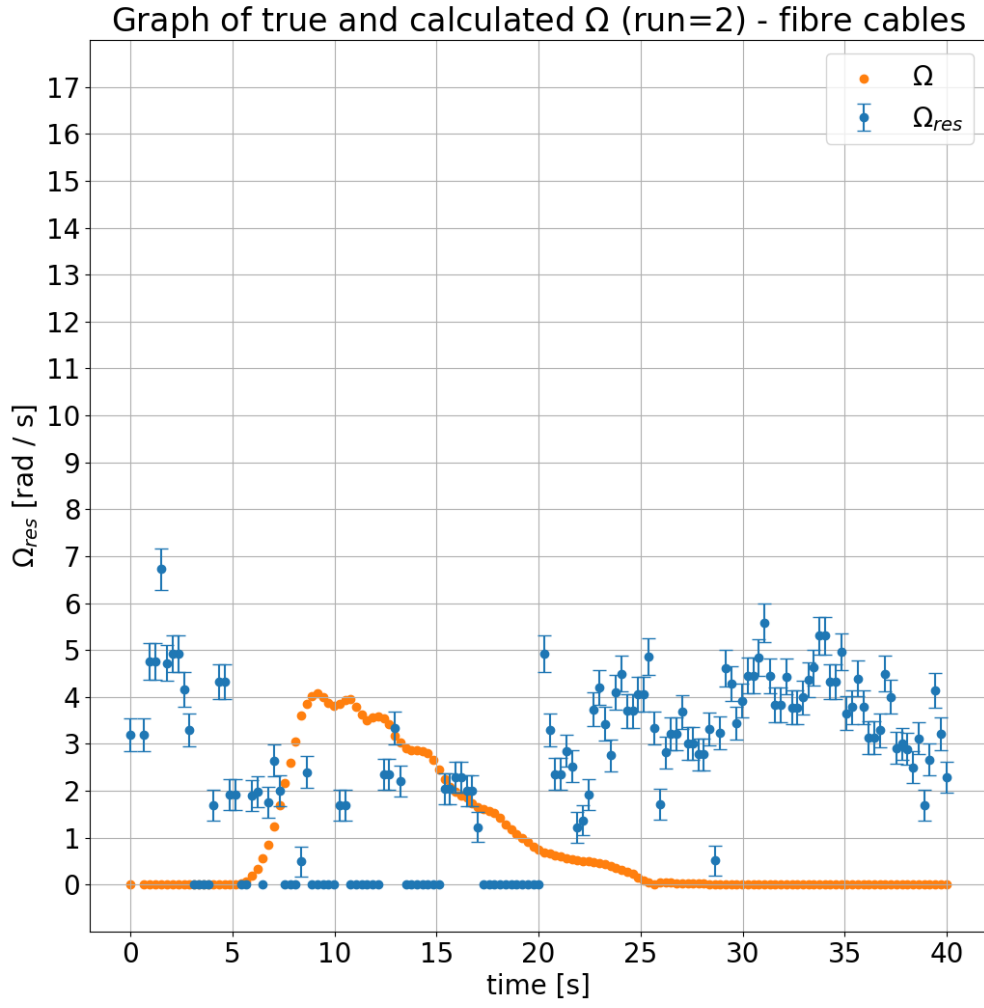
Figure 15: The comparative graph of the true omega(orange) and the omega calculated from intensity(blue) against time for run number 17 of the mirror variant.

6 Discussion

To answer our research question and find the most optimal configuration for an optical gyroscope, we researched three set-ups, testing two of them. In our results, we found that using the median absolute percentage error, the variant with the fiber-optic cables was (1.8 ± 0.6)x more accurate than the one with the acrylic tubes with a median absolute percentage error of (27 ± 6) % compared to (48 ± 5) % for the acrylic tube variant. The difference in accuracy between the two matched the theoretical prediction, of 1.68 closely, indicating the effectiveness of the median absolute percentage error in excluding outliers from the calculations. The greater accuracy of the fiber-optic variant was expected, due to the greater area enclosed by the cables compared to the one for the acrylic tubes. This was due to the shape of the fiber-optic loops which formed a circle of diameter 23.5 cm and were 1 m in total, so the light rays went through each loop approximately 1.35 times, enclosing a total effective area of 0.043 m^2. On the other hand, due to their irregular shape, the acrylic tube effectively enclosed a 10 x 10 cm square area and we approximated the number of turns to be 2.85, hence enclosing 0.029 m^2 in total, significantly less than the former setup. As indicated by equation (7), the accuracy of the interferometric gyroscope is primarily dependent on the area enclosed by the light rays. Perhaps using acrylic tubes enclosing the same area would provide similar results; however, they would be significantly harder to manufacture and more expensive. Moreover, they would be much harder to work with than fiber-optic cables due to their rigid shape and brittleness. Another possible flaw of the acrylic tubes is their large diameter, which was 1 cm. This meant that when the laser beams exited the acrylic tubes, the light was spread over a much greater area, making it less focused and it was not possible to absorb all of the laser light. It may also have led to the light waves following a range of different paths leading to varying phase differences and less effective interference. On the other hand, the fiber-optic cables had 105 μm and 125 μm diameters. Therefore, the beams that exited the cables were more focused and had a much smaller path deviation across different light rays. Finally, the use of a wired laser in the acrylic setup may have also been a source of error that reduced the accuracy of this variant. The wire of the laser was plugged into a socket above the setup such that it would spool over it and allow it to rotate. However, it still twisted during the rotation and applied torque to the laser, which may have caused its orientation to shift slightly. As a consequence, the value for the stationary light intensity, I_0 may have been different at the end than the start, influencing our calculations. Hence, it is possible that one or more of our approximations (for example the number of turns) were inaccurate. This is a possible point of improvement for the experiment that would require developing new theory or, more simply, using circular glass tubes.

On the other hand, the weighted root mean squared error shows that the error for the two setups is similar $((2.2 \pm 0.2)$ rad/s and (2.1 ± 0.2) rad/s respectively). These results are far off what we expected but are justified when considering that this error calculation method takes into account outliers. This indicates that the fiber-optic setup was influenced more by outliers caused by significant sources of error than its counterpart. The greatest source of error was changes in the background lighting. In the optics room, we were working simultaneously with other groups who were using various light sources, such as lamps or phones. While at a distance from the photo-resistor, lights were being turned on or off at random times we could not control causing variation in the light intensity measured by the component, and influencing the accuracy of our results causing random errors. For example, turning on a lamp would result in an increase in the light intensity measured by the photo-resistor, which would cause the apparent rotational velocity to be greater than in reality. This explains the deviation for some scattered data points from the true value of the rotational velocity (visible in multiple figures in the appendix). We believe the fiber-optic variant may have been affected more by such a source of error due to performing the experiment on a day when more teams were working in the optics rooms and at closer proximity. Another possible source of error for both setups is slight differences in the path traveled by the two split laser beams. For example, while we used holders, in the form of the stands for the mirror variant, to place one cable on top of the other and minimize the path difference there starting and endpoints of the lasers were different and they didn't always lie exactly on top of each other. Therefore, it is possible that there was some path difference between the two, leading to errors in the results. This may also have been the case with the acrylic tube setup due to deviations in the distances from the acrylic tubes to the photo-resistor and beam splitter respectively, causing the light rays to travel greater distances in air instead of the acrylic.

Neither setup was too complicated or took too long to construct and align, even though the alignment for the fiber-optic variant was harder to achieve as the laser beams were smaller, whilst the acrylic tubes covered the entirety of the photo-resistor by default. On the other hand, as seen in Table 3, the acrylic tube setup was more expensive to put together due to the use of the beam splitter and the cost of the green laser. It is possible we would be able to construct a functioning setup for the acrylic variant with the two red lasers, despite them being designed for use with fiber optics, however, we were unable to successfully do so due to time constraints. This would have made the cost of the two setups more similar. Even so, the advantage in the accuracy of the fiber-optic variant greatly outweighs the simplicity of the acrylic setup, making it the optimal configuration between the two. Lastly, the setup using mirrors was definitely the most difficult to align, as the laser beams

would become miss-aligned over the slightest disturbance. This was one of the main reasons, we did not manage to take any significant measurements using the mirror setup variant.

Regarding the acrylic tube setup, it was slightly unexpected that it functioned as well as it did, considering the two beams were polarized in perpendicular directions after leaving the beam splitter and no polarizing filter was used at the ends. The most likely explanation for this is that, due to the irregular shape of the acrylic tube and the total internal reflection occurring inside it, the direction of polarization of the light rays changed just enough while the beams were inside the acrylic tubes. Consequently, the two laser beams were not perpendicularly polarized and were able to interfere. Therefore, a polarizing filter turned out not to be necessary. This may have been influenced by the fact that the two acrylic tubes were identical, and mirrored copies of each other so one laser beam went through the acrylic tube in the opposite direction the other one did (w.r.t. the center of rotation). Hence, any changes in polarization occurred in the opposite order.

Finally, there were drawbacks concerning the mirror setup, evident without collecting any measurements. The most significant was the lack of a non-polarizing beam splitter, making significant data collection for the mirror variant of the gyroscope impossible. To perform the experiment effectively we would have needed a 50/50 non-polarizing beam splitter to split the beam evenly to both paths. We could have then polarized the light prior to it hitting the photo-resistor. Secondly, the alignment with the equipment we used was very time-consuming, which was expected for this variant, something that was not the case in the other variants to the same extent. Furthermore, the alignment was very sensitive and could even be broken by exerting a little pressure on the styrofoam base. Possible sources that led to the alignment being broken included any motion of the mirrors within 3D printed stands, or movement of the stands themselves, as well as due to the torque that the source wire applied on the laser, causing a slight change in the angle of emission. Some of these issues were solved by adding thin pieces of paper between the mirror stand and the mirrors to stop them from moving and duct-taping the mirror to the base. Replacing our laser with the wireless one used in the fiber-optic variant of the experiment was not an option as the laser beam spread too much when not confined in some sort of tubing. Hence, it would not have been suitable for this variant. However, since we did not have access to the non-polarizing beam splitter, the extent to which our modifications improved the setup could not be tested. Nevertheless, replicating this variant without specialized equipment does not seem optimal. However, if the trade-off in the time it takes to set up the mirror variant is justified with a significant increase in accuracy, then the mirror variant would have an upside to the other two putting it in contention for the most optimal setup. Unfortunately, we were not able to find this out.

7   Conclusion

From our results, we can conclude that overall, the fiber-optic variant is the optimal configuration of an interferometric gyroscope due to its greater accuracy. However, this is not a consequence of the Sagnac effect working better with fiberglass, rather the properties of the fiberglass make it easier to enclose a large area while taking up little space and remaining relatively cheap. Hence, it would be reasonable to conclude that the popularity of a given in material in state-of-the-art interferometric gyroscopes is dependent on how easy it is to maximize the effective enclosed area whilst taking up as little space as possible. For further improvements on the experiment, the two best ways would be having access to an isolated system (for example our own darkroom) and improvements in equipment. The dark room would help us take measurements without any unwanted light hitting the photo-resistor and affecting our results. Also, overall improvements on the equipment could be made to obtain the smallest instrumental errors possible. This could be achieved by having a motor or spinning device initiate the motion of the platform. A longer fiber-optic wire would improve the accuracy of the measurements as well since the accuracy of measuring the Sagnac effect depends on the enclosed area. This would increase sensitivity and give results closer to the actual angular velocity. Such improvements would be easy to achieve by using longer fiber-optic cables or moving the mirrors further away from the beam splitter in order to increase the enclosed area. However, it would not be ideal to use acrylic tubes due to their rigidity and brittleness. We would also benefit from having an actual optical breadboard which would allow the laser and other parts to be attached to rod bases in the breadboard, providing significantly greater stability and making the alignment easier. Due to the increased stability, we would have a much easier time constructing the mirror variant of the interferometric gyroscope which would allow us to collect more measurements. On the other hand, the optical breadboard would require the rotation mechanism to improve significantly due to the increase in the weight of the setup and the rods that would extend beneath the breadboard.

8 Sources and References

References

[1] R. Bergh, H. Lefevre, and H. Shaw, "An overview of fiber-optic gyroscopes," *Journal of Lightwave Technology*, vol. 2, no. 2, pp. 91–107, 1984.

[2] V. Passaro, A. Cuccovillo, L. Vaiani, M. Carlo, and C. Campanella, "Gyroscope technology and applications: A review in the industrial perspective," *Sensors*, vol. 17, October 2017. [Online]. Available: https://www-proquest-com.proxy-ub.rug.nl/scholarly-journals/gyroscope-technology-applications-review/docview/1965672559/se-2.doi:https://doi-org.proxy-ub.rug.nl/10.3390/s17102284.

[3] D. J. Blijleven, "Lab manual," *Physics Laboratory 1*, 8 2022.

[4] G. Sagnac, ""sur la preuve de la réalité de l'éther lumineux par l'expérience de l'interférographe tournant" [on the proof of the reality of the luminiferous aether by the experiment with a rotating interferometer]," *Comptes Rendus*, vol. 157, pp. 1410–1413, 1913.

[5] W. M. Macek and J. Davis, D. T. M., "ROTATION RATE SENSING WITH TRAVELING-WAVE RING LASERS," *Applied Physics Letters*, vol. 2, no. 3, pp. 67–68, 11 2004. [Online]. Available: https://doi.org/10.1063/1.1753778

[6] V. Vali and R. W. Shorthill, "Fiber ring interferometer," *Appl. Opt.*, vol. 15, no. 5, pp. 1099–1100, May 1976. [Online]. Available: https://opg.optica.org/ao/abstract.cfm?URI=ao-15-5-1099

[7] F. Dell'Olio, T. Tatoli, C. Ciminelli, and M. Armenise, "Recent advances in miniaturized optical gyroscopes," *Journal of the European Optical Society*, vol. 9, 2014. [Online]. Available: https://www.jeos.org/index.php/jeos_rp/article/view/14013/1170

[8] Aug 2015. [Online]. Available: https://www.raspberrypi.org/help/what-%20is-a-raspberry-pi/

[9] W. K. Burns, P. F. Liao, and P. Kelley, *Optical fiber rotation sensing.* Academic Press, 2012.

[10] D. J. Griffiths, *Introduction to Electrodynamics*, 4th ed. Cambridge University Press, 2017.

[11] ——, *Introduction to Electrodynamics*, 4th ed. Cambridge University Press, 2017.

[12] S. Dimitrijev, *Principles of semiconductor devices*, 2nd ed. Oxford University Press, 2012.

[13] Gus, "How to setup a raspberry pi light sensor," Oct 2022. [Online]. Available: https://pimylifeup.com/raspberry-pi-light-sensor/

[14] Jan 2023. [Online]. Available: https://datasheets.raspberrypi.com/sense-hat/sense-hat-product-brief.pdf

[15] K. Ellis, S. Godbole, S. Marshall, G. Lanckriet, J. Staudenmayer, and J. Kerr, "Identifying active travel behaviors in challenging environments using gps, accelerometers, and machine learning algorithms," *Frontiers in public health*, vol. 2, p. 36, 4 2014.

[16] V. R. R. Jose, "Percentage and relative error measures in forecast evaluation," *OPERATIONS RESEARCH*, vol. 65, no. 1, pp. 200–211, JAN-FEB 2017.

[17] R. G. Pontius, O. Thontteh, and H. Chen, "Components of information for multiple resolution comparison between maps that share a real variable," *Environmental and Ecological Statistics*, vol. 15, no. 2, p. 111–142, 2007.

9 Appendix

9.1 Programming

9.1.1 Measurements taking code

Link to Python code that was used to measure and process the data:
https://github.com/MartinOpat/Lab2RaspPi

9.1.2 Raw data & data processing code

Link to files containing raw data and data processing for each setup:
https://github.com/MartinOpat/Lab2RaspPi/tree/main/data

9.2 Error Propagation and Other Derivations

All the error formulas below were derived using Gauss' Law of Error Propagation [3].

9.2.1 Error propagation for Φ

$$I = I_0 \cos{(\Phi+)}^2 10$$
$$cos^2\Phi \approx 1 - \Phi^2$$
$$\Delta\Phi = \frac{\Delta I}{2\sqrt{1 - \frac{I}{I_0}}}, \ \Delta I = 0.2\% \tag{14}$$

9.2.2 Error propagation for Ω_{res}

$$\Delta\Omega_{res} = \Omega_{res}\sqrt{\left(\frac{\Delta\Phi}{\Phi}\right)^2 + \left(\frac{\Delta A}{A}\right)^2 + \left(\frac{\Delta\lambda}{\lambda}\right)^2} \tag{15}$$

9.2.3 Standard Error in the Mean [3]

$$\text{Standard error deviation: } \sigma = \sqrt{\frac{1}{N}\sum_{i=1}^{N}(x_i - \mu)^2} \tag{16}$$

$$\text{Standard error in the mean: } SE = \frac{\sigma}{\sqrt{N}} \tag{17}$$

,where N is the number of measurements, x_i is the i-th measurement and μ is the arithmetic mean of all the measurements.

9.3 Additional Graphs

9.3.1 Acrylic Tubes Variant

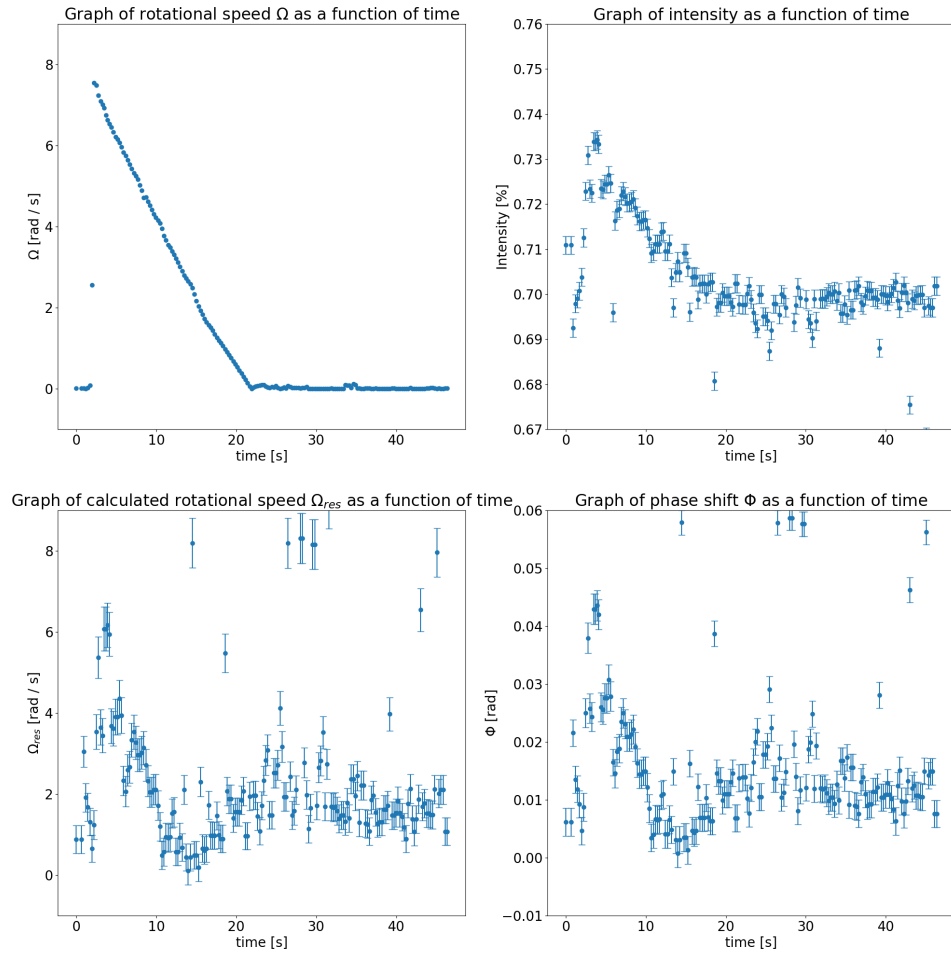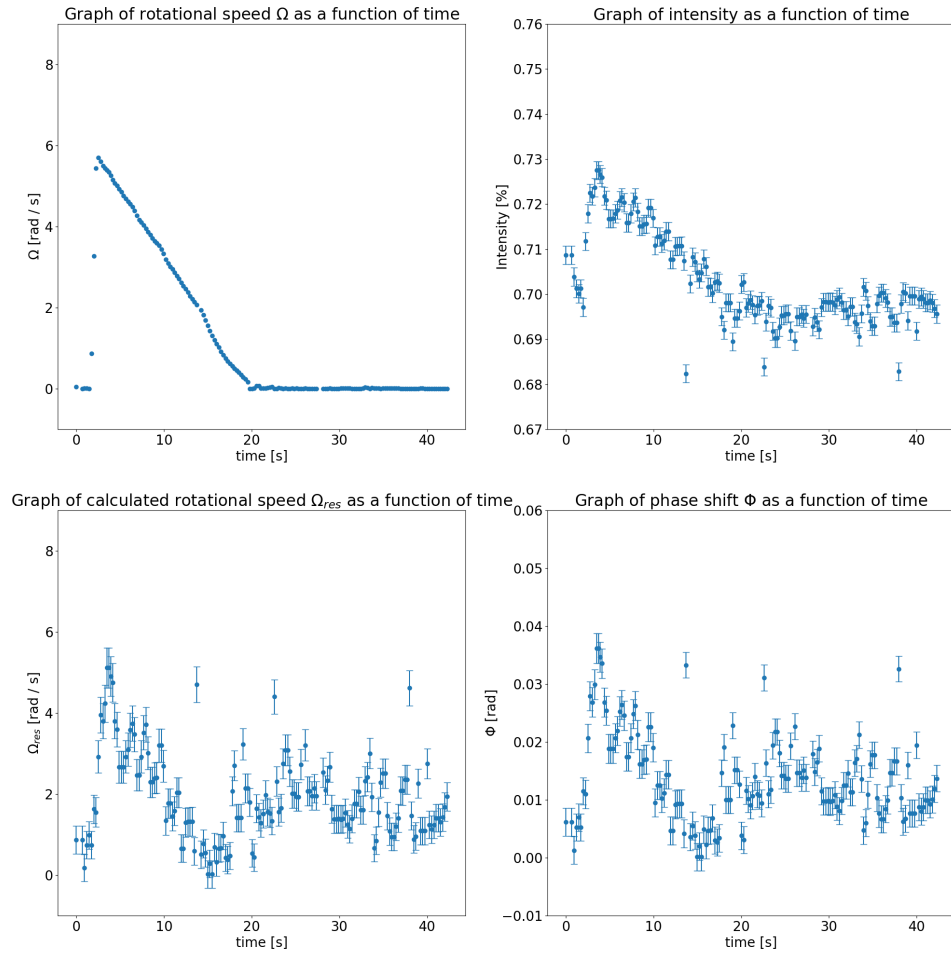Graphs for one complete measurement using acrylic-tubes setup (run=4)
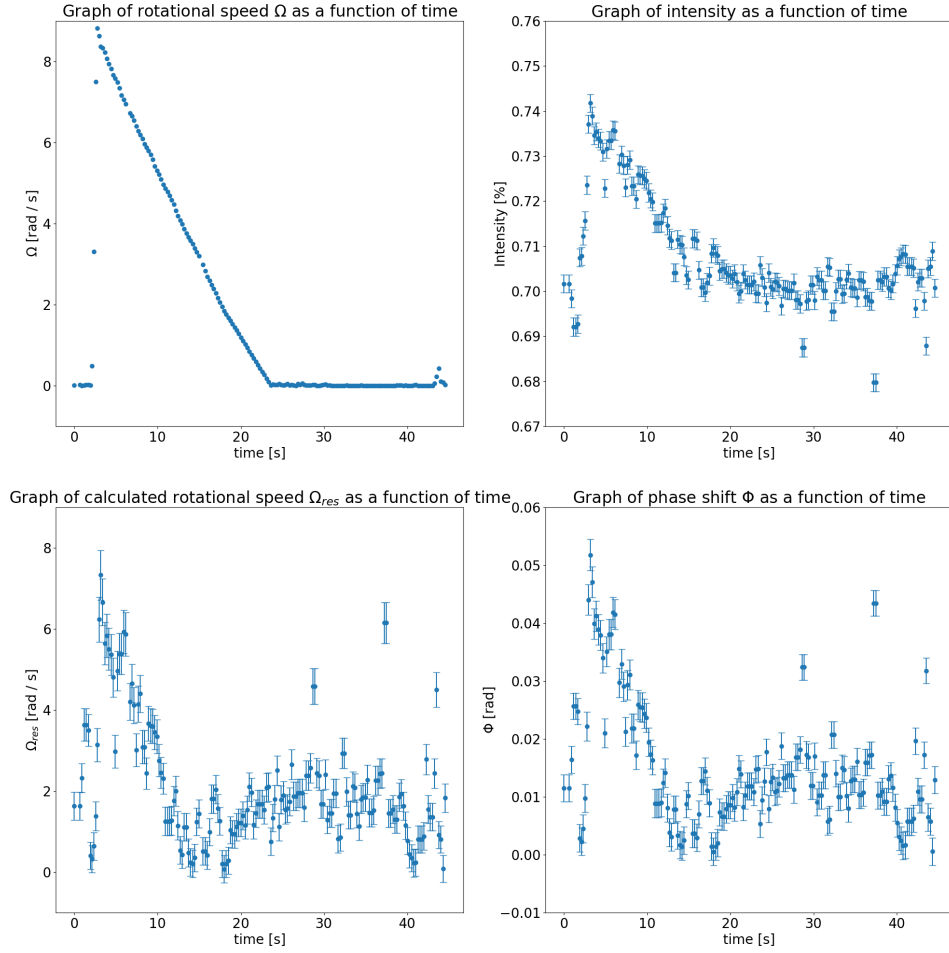
Figure 16: The graphs of rotational speed measured by the Raspberry Pi, intensity measured by the photo-resistor, rotational speed calculated from the intensity, and phase shift of the light from run number 4 of the acrylic tubes variant.

Figure 17: The graphs of rotational speed measured by the Raspberry Pi, intensity measured by the photo-resistor, rotational speed calculated from the intensity, and phase shift of the light from run number 5 of the acrylic tubes variant.
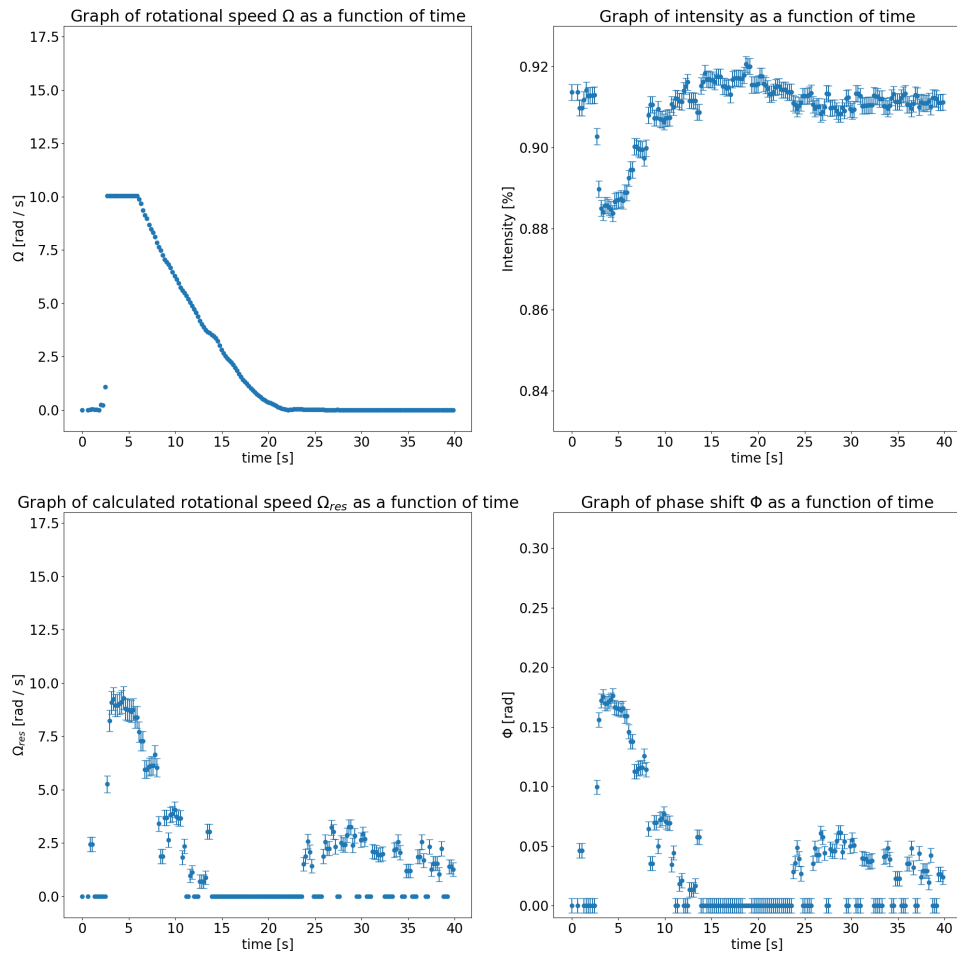
Figure 18: The graphs of rotational speed measured by the Raspberry Pi, intensity measured by the photo-resistor, rotational speed calculated from the intensity, and phase shift of the light from run number 7 of the acrylic tubes variant.
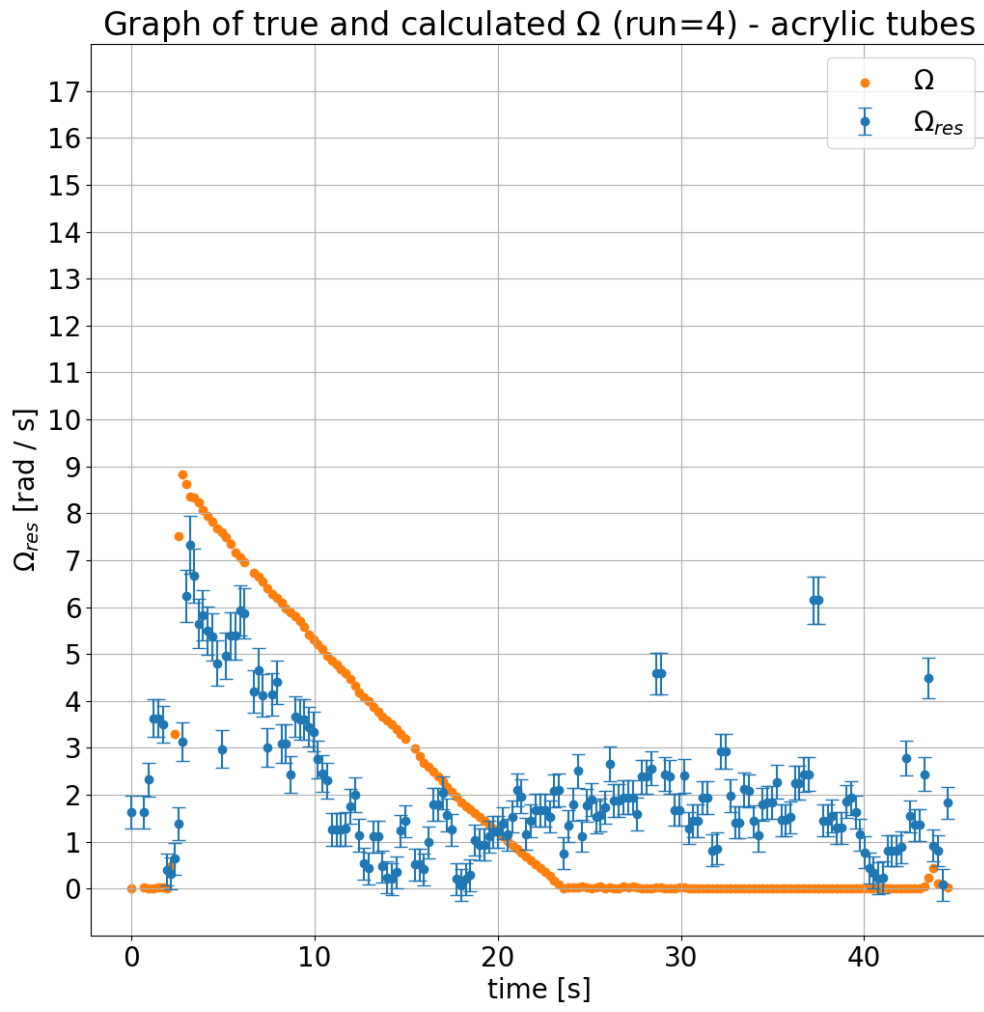
Figure 19: The comparative graph of the true omega(orange) and the omega calculated from intensity(blue) against time for the run number 4 of the acrylic tubes variant
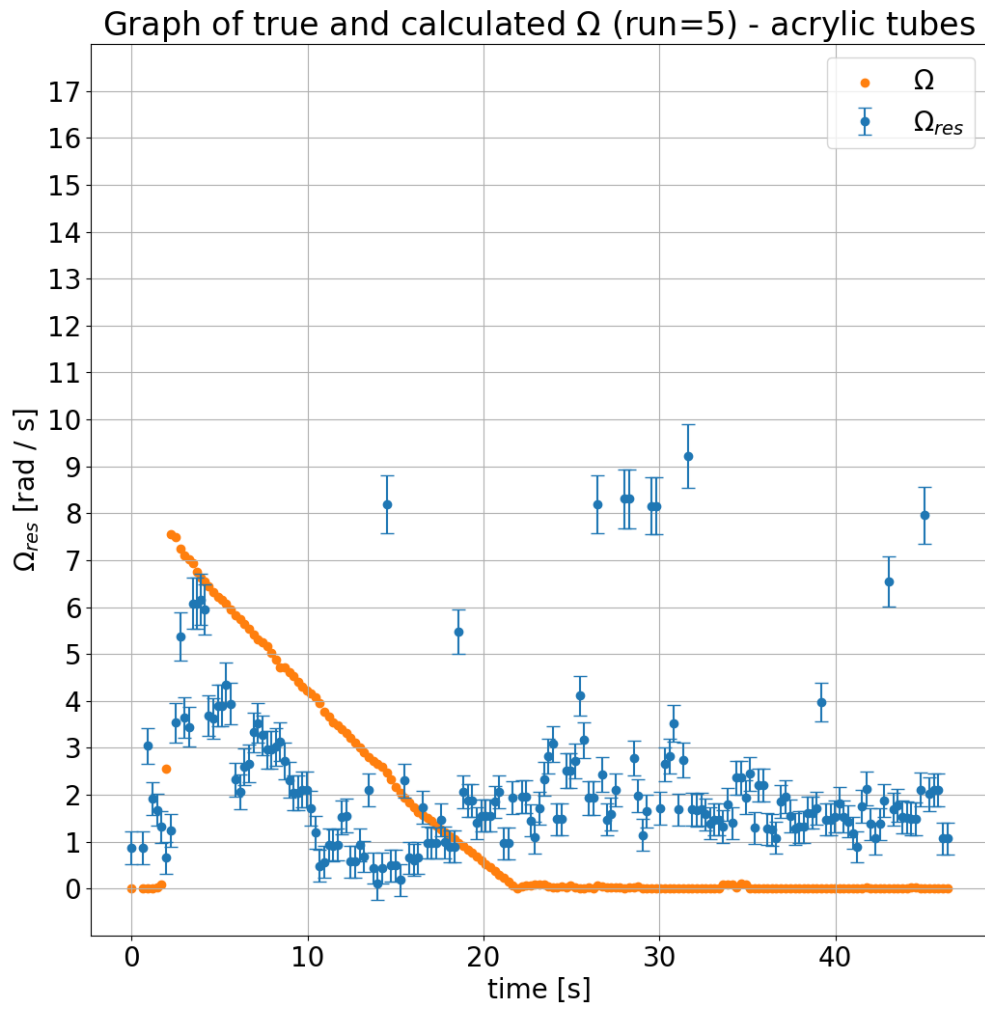
Figure 20: The comparative graph of the true omega(orange) and the omega calculated from intensity(blue) against time for the run number 5 of the acrylic tubes variant
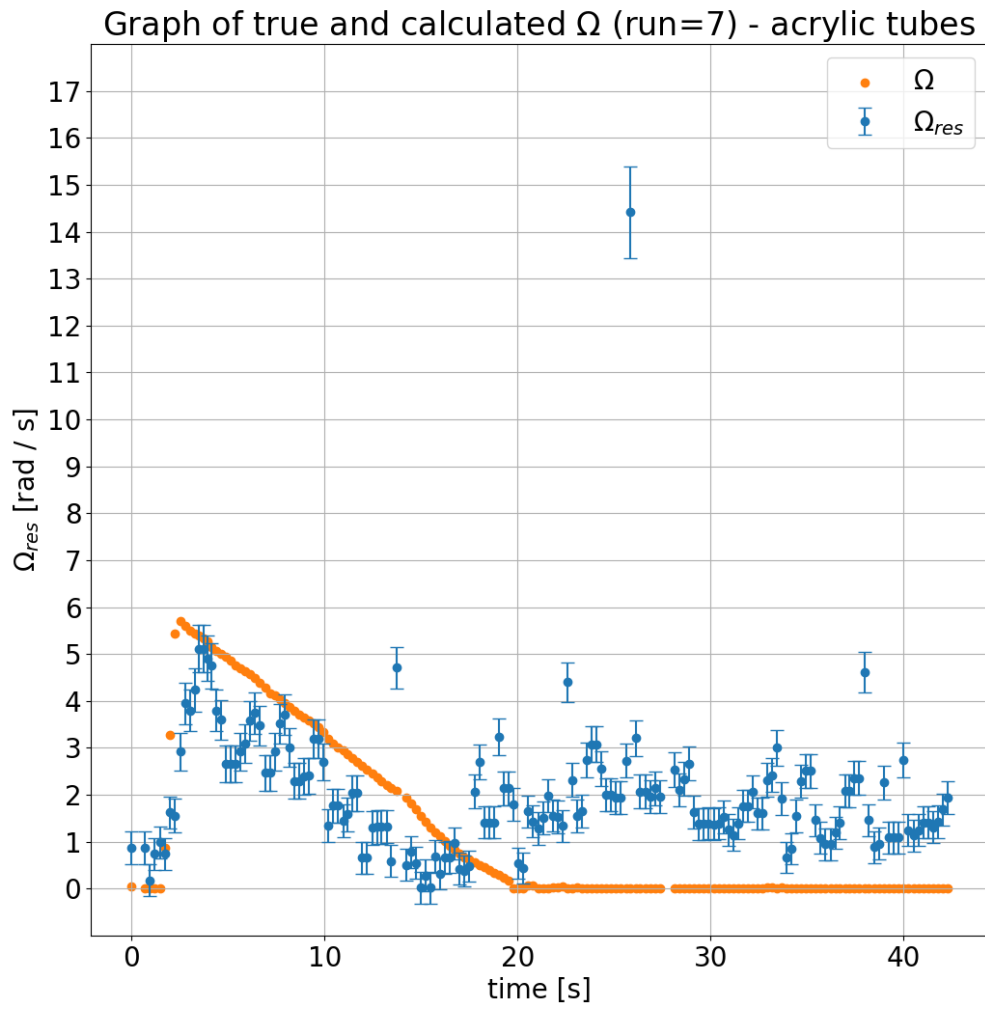
Figure 21: The comparative graph of the true omega(orange) and the omega calculated from intensity(blue) against time for the run number 7 of the acrylic tubes variant

9.3.2 Fiber-Optic Variant

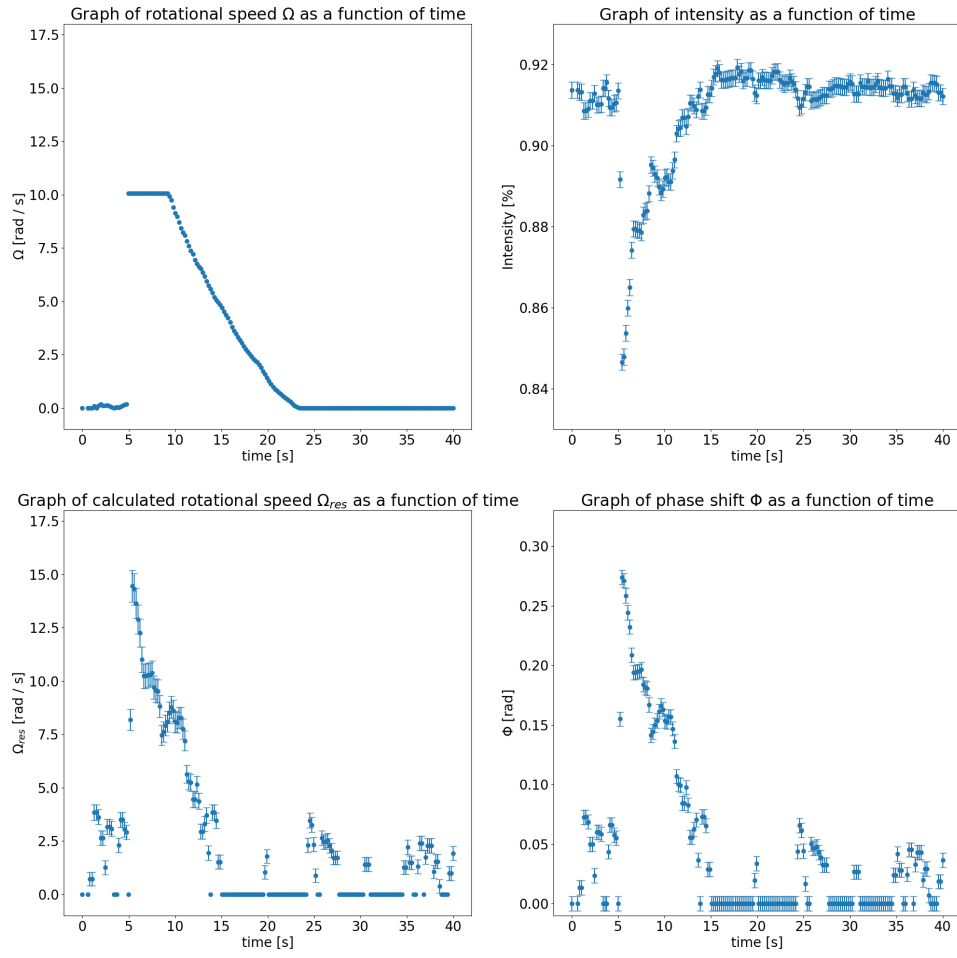Graphs for one complete measurement using fibre-cables setup (run=14)

Figure 22: The graphs of rotational speed measured by the Raspberry Pi, intensity measured by the photo-resistor, rotational speed calculated from the intensity, and phase shift of the light from run number 14 of the fiber-optic variant.

Figure 23: Graphs of rotational speed measured by the Raspberry Pi, intensity measured by the photo-resistor, rotational speed calculated from the intensity, and phase shift of the light from run number 17 of the fiber-optic variant.
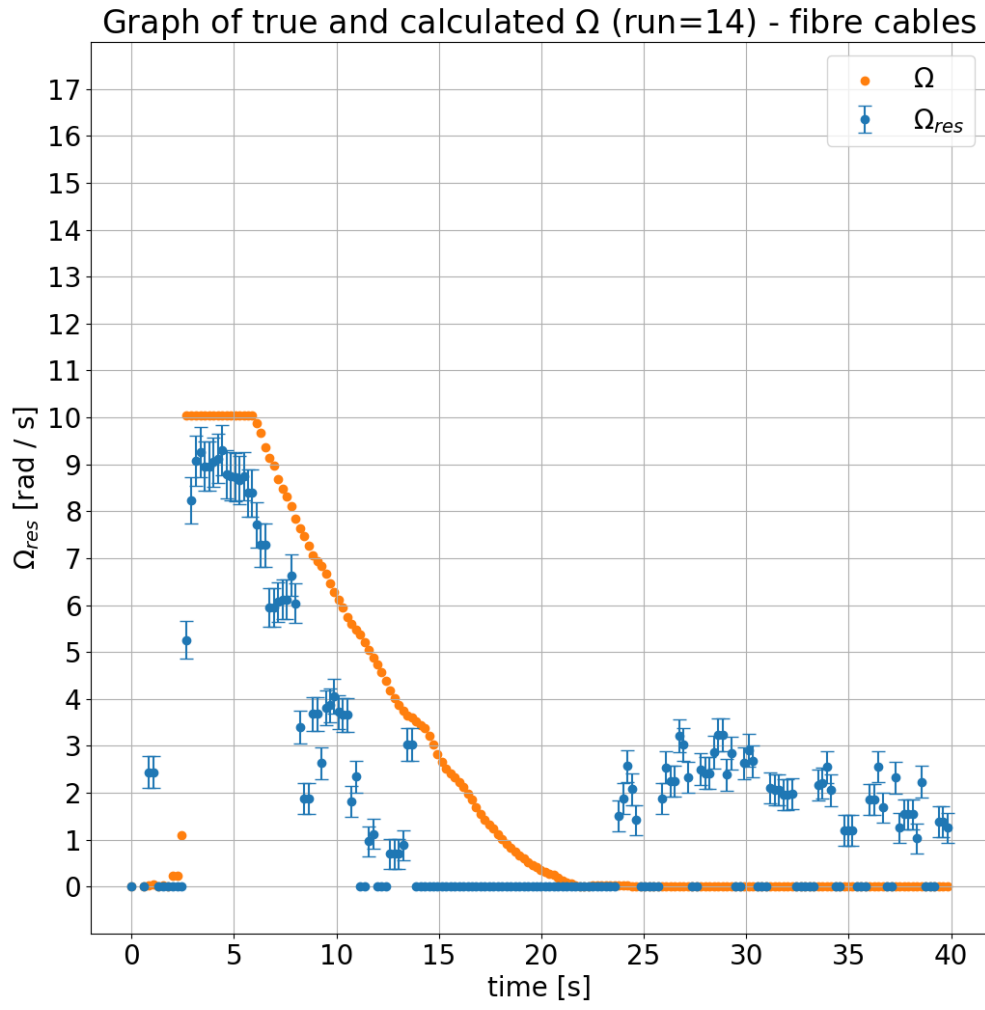
Figure 24: The comparative graph of the true omega(orange) and the omega calculated from intensity(blue) against time for the run number 14 of the fiber-optic variant.
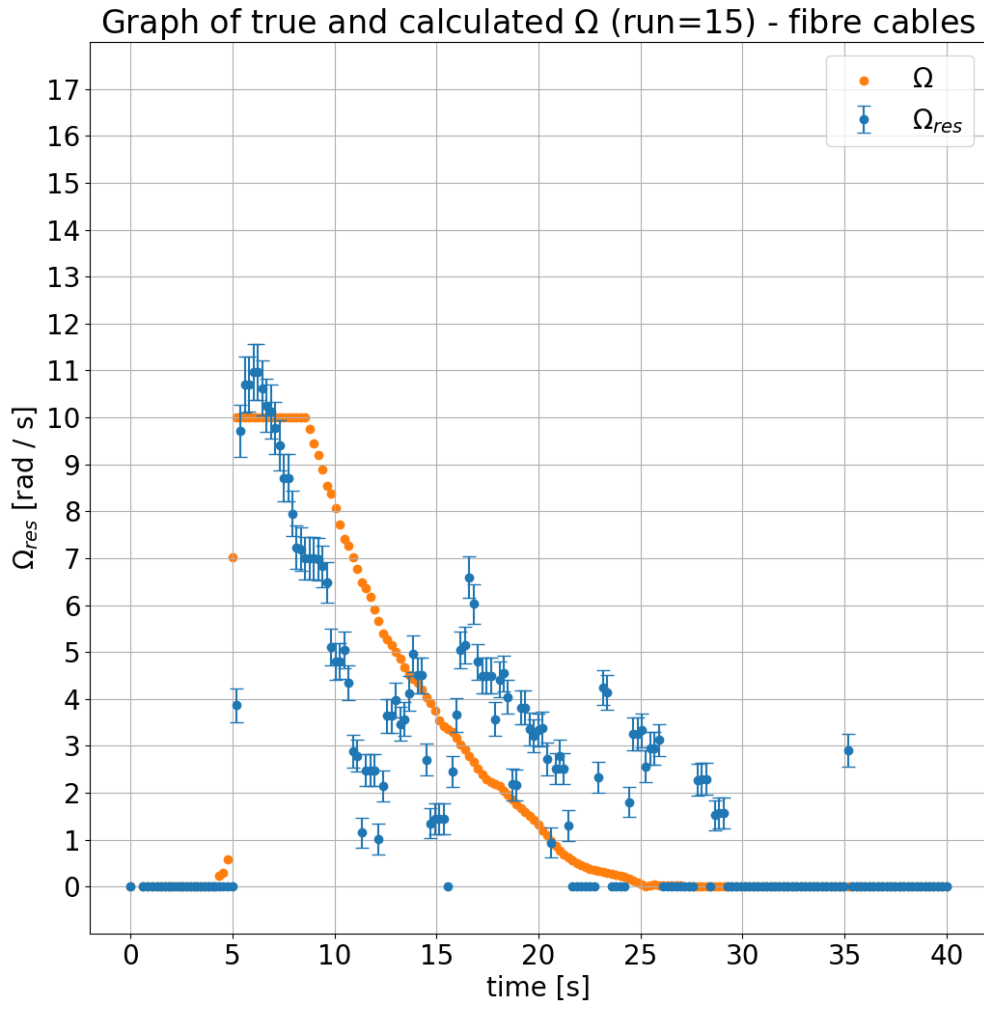
Figure 25: The comparative graph of the true omega(orange) and the omega calculated from intensity(blue) against time for the run number 15 of the fiber-optic variant.
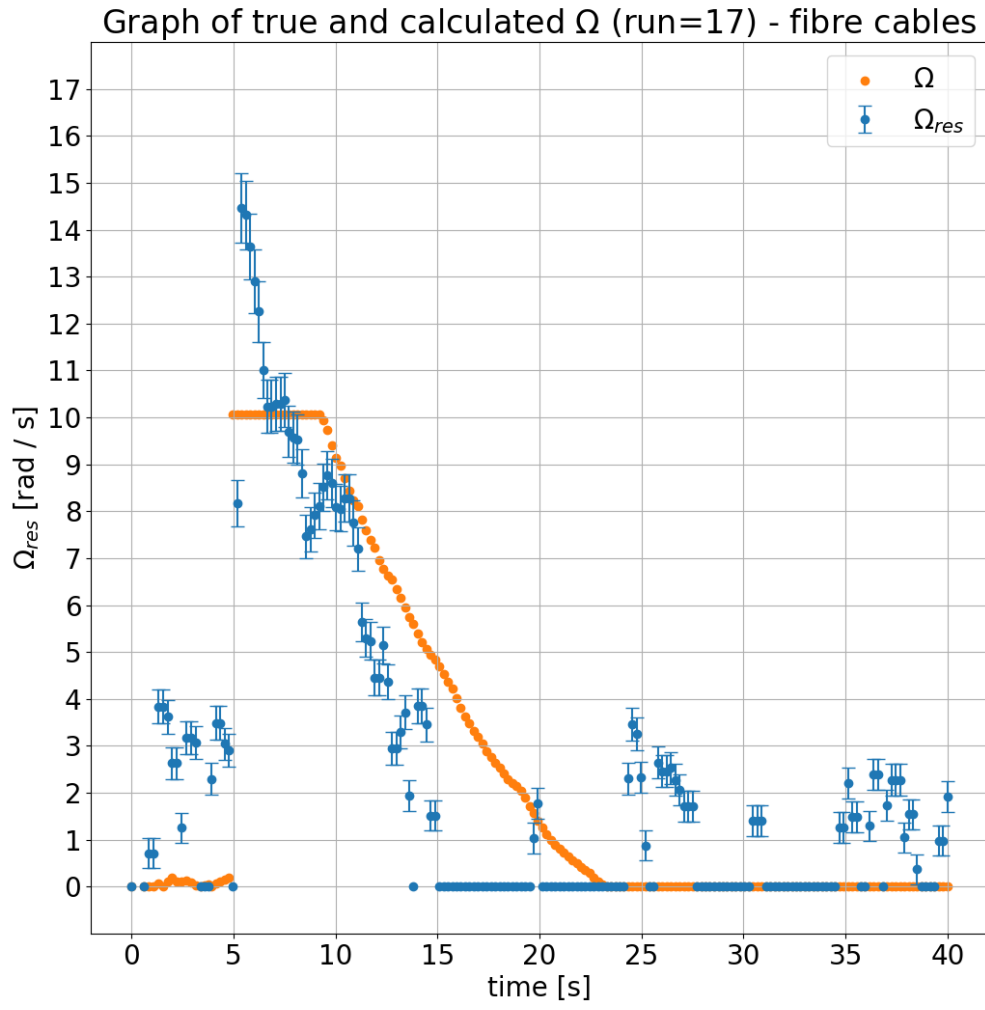
Figure 26: The comparative graph of the true omega(orange) and the omega calculated from intensity(blue) against time for the run number 17 of the fiber-optic variant.